Structural performance of flexible freeform panels subjected to wind loads

2 Yong Yoo¹, Zaryab Shahid², Renzhe Chen³, Maria Koliou⁴, Anastasia Muliana⁵, Negar Kalantar⁶

3 ABSTRACT

An increased number of hurricanes and tornadoes have been recorded worldwide in the last decades, while research efforts to reduce wind-related damage to structures become essential. Freeform architecture, which focuses on generating complex curved shapes including streamlined shapes, has recently gained interest. This study focuses on investigating the potential of kerf panels, which have unique flexibility depending on the cut patterns and densities, to generate complex shapes for facades and their performance under wind loads. To investigate the kerf panel's potential capacity against wind loads, static and dynamic analyses were conducted for two kerf panel types with different cut densities and pre-deformed shapes. It was observed that although solid panels result in smaller displacement amplitudes, stresses, and strains in some cases, the kerf panels allow for global and local cell deformations resulting in stress reduction in various locations with the potential to reduce damage due to overstress in structures. For the pre-deformed kerf panels, it was observed that both the overall stress and strain responses in kerf cut arrangements were lower than those of the flat-shaped panels. This study shows the promise of the use of kerf panels in achieving both design flexibility and performance demands when exposed to service loadings. Considering

¹ Former Ph.D. Student, Zachry Dept. of Civil and Environmental Engineering, Texas A&M University, College Station, TX, 77843, U.S.A., email: yongyoo8958@tamu.edu

² Former Ph.D. Student, J. Mike Walker '66 Dept. of Mechanical Engineering, Texas A&M University, College Station, TX, 77843, U.S.A., email: zaryab94@tamu.edu

³ Former M.S. Student, J. Mike Walker '66 Dept. of Mechanical Engineering, Texas A&M University, College Station, TX, 77843, U.S.A., email: crzhust@163.com

⁴ Associate Professor, Zachry Dept. of Civil and Environmental Engineering, Texas A&M University, College Station, TX, 77843, U.S.A., email: maria.koliou@tamu.edu (corresponding author)

⁵ Linda & Ralph Schmidt '68 Professor, J. Mike Walker '66 Dept. of Mechanical Engineering, Texas A&M University, College Station, TX, 77843, U.S.A., email: amuliana@tamu.edu

⁶ Associate Professor, Architecture Division, California College of the Arts, San Francisco, CA 94107, U.S.A., email: <u>kalantar@cca.edu</u>

that this newly proposed architectural configuration (design paradigm) for façades could revolutionize structural engineering by pushing complex freeform shapes to a standard practice that intertwines aesthetic arguments, building performance requirements, and material design considerations has the potential for significant practical applications.

Keywords: freeform structure, kerfing method, wind load analysis, cladding component

1 Introduction

18

19

20

21

22

23

24

25

26

27

28

29

30

31

32

33

34

35

36

37

38

39

40

41

Natural hazards, such as earthquakes, tsunamis, hurricanes, and flooding, threaten many communities in the United States and around the world every year, resulting in infrastructure damage often associated with significant fatalities and billions of dollars in economic losses (Simmons et al., 2013; Reeves, 2015; Boustan et al., 2020; Koliou and van de Lindt, 2020; Raker, 2020)015;Boustan et al., 2020;Koliou and van de Lindt, 2020;Raker, 2020). According to the National Oceanic and Atmospheric Administration (NOAA), the number of incidents of windrelated hazards has steadily increased since 1995 (NOAA, 2020b;c). More specifically, based on the data provided by the United States Environmental Protection Agency (EPA), hurricanes and tropical storms encountered in the Atlantic (EPA, 2016) and East Pacific basin were constantly grown (NOAA, 2020b), while an average annual tornado count of 1,251 was observed in the United States between 1950 and 2019 (NOAA, 2020c). As shown in Fig. 1, the number of tornadoes has been maintaining an upward trajectory since 2014, with 2019 being the top five years of tornadoes in the United States since 1950. Although the total number of hurricanes that struck the United States in each decade classified per the Saffir-Simpson Categories has decreased since 1950, the total number of hurricane occurrences classified as Category 3 and higher has increased (see Fig. 2) (Blake et al., 2005).

Such an increased trend in wind-induced disasters can lead to significant economic losses to our society (Simmons et al., 2013;Reeves, 2015;NOAA, 2020a) and result in human injuries or

fatalities (Simmons et al., 2013; NOAA, 2022). Several studies available in the last few years have focused on estimating and assessing the damage due to wind-induced loads by performing risk (Standohar-Alfano and van de Lindt, 2016; Koliou and van de Lindt, 2020), benefit-cost (Simmons et al., 2015; Simmons et al., 2020), statistics (Reeves, 2015; Raker, 2020), and fragility (Amini and van de Lindt, 2014) analyses. Furthermore, many studies have investigated methods and solutions (Doan and Nguyen, 2019; Ta and Tran, 2020; Dung et al., 2021; Phung et al., 2022), including energy dissipation and structural response reduction methods, at the building-design level to alleviate such impacts on infrastructure systems and communities. Existing approaches commonly used to mitigate energy from high-velocity winds include increasing stiffness (Chan et al., 2010; An, 2016), building mass (Chen and Chui, 2017), as well as using damping devices (Saaed et al., 2015; Jafari and Alipour, 2020). Meanwhile, there is a growing interest in the construction of freeform architectural structures incorporating complex shapes compared to existing conventional structural shapes (Pottmann et al., 2007; Eigensatz et al., 2010; Ha et al., 2014; Eekhout, 2016; Pottmann and Wallner, 2016; Andrade et al., 2017; Son et al., 2017). Freeform structures have not only a unique building shape that incorporates curved and flexible patterns, but also a streamlined shape that can change the flow of wind patterns (Mooneghi and Kargarmoakhar, 2016; Sharma et al., 2018), and therefore could be impactful in the performance of structural systems subjected to extreme wind loads. Panel and cladding components used to develop the shape of such freeform structures were considered both "flat" panels and "pre-deformed" panels with initial curvature (deflection). It is quite challenging and costly to manufacture complex freeform-shaped panels out of conventional construction materials, such as steel, concrete, aluminum, glass, and wood (Eigensatz et al., 2010; Kim et al., 2015). Regarding the problems of the manufacturing process and cost, Eigensatz et al. (2010) studied a method of controlling the overall cost by producing multiple panels using

42

43

44

45

46

47

48

49

50

51

52

53

54

55

56

57

58

59

60

61

62

63

64

mold fabrication. Kim et al. (2015) also studied the performance of freeform concrete panels by comparing manageable production costs and time with existing construction materials focusing mainly on production time and worker productivity. Son et al. (2017) investigated freeform concrete curved panels at the material level to obtain an efficient production process in terms of cost, workability, and durability. It is worth noting that all these studies ((Eigensatz et al., 2010), (Kim et al., 2015), (Son et al., 2017)) dealt with rigid solid freeform curved panels.

66

67

68

69

70

71

72

73

74

75

76

77

78

79

80

81

82

83

84

85

86

87

88

89

One of the practical approaches for constructing a flexible panel for freeform structures is a relief cutting or kerfing method. Recently conducted studies on the kerfing technique focused on wood kerf panels and particularly the effect of cut patterns as well as unit components' sizes that can affect local stiffness and overall curvature (Kalantar et al., 2016;Guzelci et al., 2017; Zarrinmehr et al., 2017; Chen, 2018; Holterman, 2018; Chen et al., 2020). Overall, the kerf panels appear to be able to generate complex freeform geometries and have the potential to tune wave propagation phenomena established on the panel surfaces by external dynamic events. Depending on the type of unit cells that make up the kerf panel and the arrangement of the panel, the kerf panel can be designed to reduce the stress response within the panel when exposed to external loads. Therefore, the kerf panels are promising for constructing freeform structures, having the advantage of simultaneously securing aesthetic beauty as well as excellent mechanical performance under external wind-induced loads. Holterman (2018) studied flexible kerf panels using plywood accounting for the advantageous features of the pattern materials including cost efficiency, availability, ability to be easily shaped, lightweight properties, and surface roughness finish. This study concluded that bending and torsion of the segment of the panel can be controlled locally depending on the type and arrangement of the patterns constituting the kerf panel. Considering these characteristics, it is possible to manufacture a kerf panel that is reconfigurable to various complex shapes. Chen et al. (2020) conducted a systematic study of kerf unit-cell and

panels by performing both analytical and experimental studies to evaluate the stretching, bending, and twisting responses of two types of kerf pattern panels, namely square and hexagon, as well as various cutting densities as shown in Fig. 3. They showed that the deformation mechanism of the kerf panel allows designing a complex shape according to the engineer's intention. Recently, Shahid et al. (2022b) investigated the dynamic responses of kerf unit cells out of wood and stainless steel and showed that the kerf cells delayed the stress wave propagation and reduced the stress amplitude (Shahid et al., 2021). Based on their understanding of the dynamic responses of kerf unit cells, Shahid et al. (2022a) further studied the dynamic responses of reconfigurable large kerf panels in terms of modal response and stress propagation. This study showed that the flexibility of the kerf panels enables local and global shape reconfigurations, which can alter the dynamic response of the kerf panels in a desired manner. Moreover, the wood kerf cell also showed energy dissipation owing to its viscoelastic characteristics (Darnal et al., 2021).

2 Scope

The scope of this study is to numerically evaluate the structural performance of kerf panels subjected to wind loading and quantify their performance compared to conventional construction methods (i.e., solid panels). To do so, two kerf panels of a square kerf pattern having different kerf cut density arrangements namely panels A and B, were considered (see Fig. 4). Panel A has a low-density cut in the mid-section of the panel and high-density cuts towards the four corners, while Panel B has a high-density cut in its center and low-density cuts towards its boundary edges. The medium-density cut was used in the transition regions from the low-density to high-density in both panels. Flat panels were first analyzed under wind loads. Next, panel A and panel B were deformed into a dome shape with different degrees of curvature. Responses of the deformed-shaped panels under wind loads were examined.

The evaluation of the performance for each panel was performed by computing response parameters including displacement (out of plane), stress (von Mises), and strain (in-plane maximum), and comparing the response of kerf panels with conventional solid panel construction. The conventional solid panel was used to be a reference model to account for the performance of the kerf panel in terms of the structural demands. This reference model has the same dimensions as the kerf panel (381 mm-by-381 mm with 3.175 mm depth) and material properties. Static and dynamic wind loading conditions were applied to each model generated in the ABAQUS software (SIMULIA, 2018) based on the ASCE 7-16 (ASCE, 2016) as well as experimental data of wind simulated loads available in the literature (He et al., 2018). The calculated static wind load condition based on the ASCE 7-16 was assumed to account for the cladding member of a low-rise building in south Texas. According to the literature (He et al., 2018), the storm duration effect should be considered when the building damage state is investigated whether the lower wind speed can damage the structure given a certain intensity of the hurricane. Thus, the dynamic loading profile was derived by multiplying the wind pressure coefficient data by the design wind pressure to account for the wind duration effect similar to the He et al. (2018) experiments performed using Louisiana State University (LSU) aerodynamic database. It should be noted that due to the lack of experimental data for the new type of façade considered (kerf panel configurations), the database obtained through the wind tunnel test of LSU was adopted for this proof-of-concept study. The following sections are organized to describe the finite element models considered in this

113

114

115

116

117

118

119

120

121

122

123

124

125

126

127

128

129

130

131

132

133

134

135

136

study (section 3), and wind loading conditions adopted (section 4) as well as present the response analysis results (section 5) in terms of modal analysis, and static and dynamic analysis. The results are presented comparatively between flat kerf panels, pre-deformed kerf panels as well and conventional solid panels. Finally, major discussion points and conclusions are presented in this manuscript (section 6).

3 Finite element models

137

138

139

140

141

142

143

144

145

146

147

148

149

150

151

152

153

154

155

156

157

158

159

The finite element models considered in this study for the kerf panels were initially developed by Chen et al. (2020) to study the mechanical behavior of various configurations of kerf panels. In addition to the kerf panel models, a solid panel model was developed to compare the responses of the kerf panels with conventional construction materials when exposed to wind loading. Each computational panel model was developed in the ABAQUS commercial software. In the following sections, descriptions of the various models considered in this study are provided.

3.1 Kerf panel models

In this paper, both flat panels A and B (as shown in Fig. 4) were generated with dimensions of 381 mm-by-381 mm and consisted of two-node beam elements (B31 in ABAQUS), i.e., panel A (110,017 elements) and panel B (136,253 elements). Geometric nonlinearity effects (NLgeom in ABAQUS) were incorporated to represent the flexibility of the kerf panels. Since high-speed wind loadings will be applied to the model, a small (under 7.62 E-03 mm) mesh size of the kerf model was used to achieve good computational accuracy based on sensitivity studies conducted comparable to Chen's model (Chen et al., 2020). Because the kerf panels are commonly crafted using the relief cutting method cutting a piece of an area using a jigsaw or laser cutting through the panel's full depth from a whole wood plate, the kerf panel model consisted of continuous beam elements to represent the construction process. Based on the arrangement of the unit-cells of the kerf pattern plane, each panel has three different types of unit-cells that have 25.4 mm-by-25.4 mm dimensions, namely high cut, medium cut, low cut density, as shown in Fig. 5. The dimensions of each unit cell and the calculated effective area for both kerf panel models are summarized in Table 1. Because the size of the kerf panel model considered in this study is smaller than what is typically used in buildings, the values of material properties were modified utilizing similitude

analysis (described in detail in Section 4). Edge-fixed boundary conditions (as shown in Fig. 6) were applied to all models. In the dynamic analysis, the damping effect was considered using Rayleigh's damping theory. It should be noted that the finite element models for both panels A and B were validated with experiment test data performed by the research team. Chen et al. (2020) conducted uniaxial, biaxial, and bending tests on the unit-cell specimens (25.4 mm-by-25.4 mm) as well as bending tests on the kerf panel (381 mm-by-381 mm) configuration. Based on the observed force and displacement data, the finite element kerf panel model was validated and further used for the scope of this study to conduct static and dynamic loading analyses.

3.2 Solid panel model description

The solid panel model, of the same dimensions (381 mm×381 mm×3.175 mm) as the kerf panels, was generated for performing the comparison study in terms of structural response, however, the solid panel model was developed using shell elements. To evaluate critical parameters influencing the accuracy of the structural analysis results, a parametric study was performed accounting for the mesh size and element type variations. More specifically, two types of mesh sizes were assigned, including 12.7 mm and 1.5875 mm, as well as two different element types including a 4-node (S4R in ABAQUS) and an 8-node (S8R in ABAQUS) element, resulting in three case models as follows: (1) mesh size 12.7 mm and S4R elements, (2) mesh size 1.5875 mm and S4R elements, and (3) mesh size 1.5875 mm and S8R elements. Based on this parametric study, it was found that the mesh size of 12.7 mm combined with S4R elements resulted in the most accurate and computationally inexpensive models (achieving accuracy by avoiding convergence error and reducing computational costs). The mechanical properties of Medium-density fiberboard (MDF), as well as boundary conditions and Rayleigh damping similar to the kerf panel models, were adopted for the solid panel model.

4 Wind loading

183

184

185

186

187

188

189

190

191

192

193

194

195

196

197

198

199

200

201

202

203

204

205

206

The wind loading conditions in this study were defined assuming a low-rise building and using standard code including the ASCE 7-16 (ASCE, 2016) wind load provisions. Due to the limitation of the experimental data of a building consisting of kerf panels (new design paradigm for facades), the database obtained through the wind tunnel test of Louisiana State University (LSU) (He et al., 2018) was used to calculate the time history wind load series for performing the dynamic analyses. The derived static and dynamic wind loads were divided by the number of nodes comprising the computational panel models and assigned concentrated loads as equivalent wind pressure to all the nodes. Since the calculated loads using codes or standards refer to solid-state members, for each kerf pattern panel, the effective area was calculated and the area ratio that is between kerf and solid panels was applied to the computed wind pressure. A cut or hole area of the panel cannot resist the wind loads and can flow the external wind-related load to the outside (Finn, 2017;2018). Therefore, the calculated effective area of each kerf pattern panel was computed as shown in Table 1 depending on the type and configurations according to the cutting densities of unit-cells that make up each kerf panel shown in Fig. 5. The effective area for the solid panel was computed to be equal to 145,161 mm² (381 mm×381 mm) assuming that all of the faces can be forced on the windrelated load. The size of the members used in this study is relatively small compared to the panel normally

The size of the members used in this study is relatively small compared to the panel normally utilized in a low-rise building's structural elements. Thus, a similitude analysis was performed to account for the material properties and effective area of each model (Harris and Sabnis, 1999;Zhu et al., 2017;Casaburo et al., 2019). From the similitude analysis, the mechanical properties of Medium-density fiberboard (MDF) were considered to model the kerf panels with a modulus of elasticity (MOE) of 390.52 MPa, Modulus of rupture (MOR) of 3.50 MPa, and Poisson's ratio of 0.25 (Chen et al., 2020). To calculate the material properties and loading conditions of the models

207 (381 mm×381 mm), actual structural panel sizes for typical low-rise building wall elements 208 (1,219.2 mm×1,219.2 mm) were used as the prototype domain model. Similitude analysis was 209 performed accounting for the three selected independent scale factors to be: length (λ_L) =3.2, time 210 $(\lambda_t) = 1$, and mass density $(\lambda_D) = 1$. Then, the scale factors for the weight (λ_w) , mass (λ_m) , stress 211 (λ_{σ}) , strain (λ_{ε}) and modulus of elasticity (λ_{E}) were computed per equations (1) - (5).

$$\lambda_{W} = \frac{\lambda_{D} \lambda_{L}^{4}}{\lambda_{i}^{2}} \tag{1}$$

$$\lambda_m = \lambda_D \lambda_L^3 \tag{2}$$

$$\lambda_{\sigma} = \frac{\lambda_{D} \lambda_{L}^{2}}{\lambda_{t}^{2}}$$

$$\lambda_{\varepsilon} = 1$$
(3)

$$\lambda_{\varepsilon} = 1 \tag{4}$$

$$\lambda_E = \frac{\lambda_D \lambda_L^2}{\lambda_t^2} \tag{5}$$

- 212 Table 2 summarizes the model and prototype domain properties based on the similitude 213 analysis.
- 214 The static wind loading conditions were implemented in all models using the load evaluation methodology as proposed by ASCE 7-16 per equations 6 and 7. 215

$$q_z = 0.613K_zK_{zt}K_dK_eV^2 (N/m^2) (6)$$

216 where, q_z = velocity pressure at height h, K_z = velocity pressure exposure coefficient, K_{zt} = topographic factor, K_d = wind directionality factor, K_e = ground elevation factor, and V = basic 217 218 wind speed.

$$p = q_h [(GC_p) - (GC_{pi})] \qquad (N/m^2)$$
(7)

where p = design pressure at the desired height, $q_h =$ velocity pressure evaluated at mean roof 219 height h, GC_p = external gust + pressure coefficient, and GC_{pi} = internal gust + pressure 220 221 coefficient.

The environment was assumed to be for low-rise buildings in the College Station, Texas region to derive each coefficient required for the load calculations. According to the assumed environment, the surface roughness, and exposure category B, a velocity pressure exposure coefficient (K_z) of 0.85 was identified. The topographic factor (K_{zt}) was assumed equal to 1 since there is no information given about the geometric area condition. The wind directionality factor (K_d) was selected to be 0.85 because the outer components of the building (e.g., panel or cladding) were selected as the structural members in this study. The ground elevation factor (K_e) is 0.9978 considering the height (18.29 m), which is the criteria for low-rise buildings. It was also assumed that the panel was installed on the wall of the low-rise building to account for the gust effect acting inside and outside of the structure by external wind loads. The basic wind speed (V) corresponding to Risk Category III in the area was computed as equal to 51.41 m/s. ASCE 7-16 also describes the wind loading conditions using the Saffir-Simpson hurricane scale reflecting the 3-s gust wind effect at 10m above open ground in the exposure category. For this study, the Saffir-Simpson hurricane scale was used to evaluate the response of the structural panels and account for extreme wind loads. To cover a wide range of wind loading conditions per the Saffir-Simpson hurricane scale categories, wind load conditions were generated at 6.71 m/s intervals varying from 35.76 m/s to 82.70 m/s. Finally, the calculated wind pressure was multiplied by a load factor of 0.6 considered in the load combination for available stress design per ASCE 7-16, however, this is recognized as a limitation of this study and LRFD factors are recommended to be considered in future studies to reflect the design considerations. To take into account the dynamic wind pressure P(t), that changes over time per equation 8, the basic wind speed was multiplied by the density of air and the fluctuating wind pressure

coefficient $(C_n(t))$, which is a function of time and can be obtained from Louisiana State

222

223

224

225

226

227

228

229

230

231

232

233

234

235

236

237

238

239

240

241

242

243

University (LSU) aerodynamic database. For the considered wind load data from the LSU database, the dynamic pressure at the storm condition was considered as an open terrain atmospheric boundary with roughness length z_0 of 0.0142m about the enclosed 1:50 scale tested building (18.3 m-by-13.4 m with overhang height of 3.0m). The test section of 2.44m in length, 1.32m in width, and 0.99m in height and it is powered by a 2.4m diameter fan. This scaled model was mounted with 192 pressure taps (188 external taps and 3 internal taps) and connected to Scanivalve DSA3217/16Px (Serial#2100), a pressure acquisition system at a sampling rate of 500 Hz for 1 hour in full scale (He, 2018). In the case of this study, *due to the lack of experimental data for the new type of façade considered (kerf panel configurations)*, the database obtained through the wind tunnel test of Louisiana State University (LSU) was adopted. The ($C_p(t)$) was referred to the literature (He et al., 2018) and was the normalized wind pressure coefficient value so it is not related to the specific effective area of the building component. The calculated time history wind pressure loading was applied to the model using an equivalent force load to the kerf panel similar to the static analysis per equation 8.

$$P(t) = 0.5 \times \rho \times V^2 \times C_p(t)$$
 (8)

where, ρ = the density of air, V = basic wind speed at the desired height, and $C_p(t)$ = the fluctuating wind load coefficient.

The wind pressure coefficient database for the low-rise buildings was built through a scale model experiment. In this study, the wind tunnel experiment database developed by Louisiana State University (He et al., 2018) was utilized to account for the panels' response. According to He et al. (2018), the vulnerability of the building to the extreme wind load increased by over 50% due to the duration effects accounted for in the study. To further account for duration effects in the

present study, a 2-second sample yielded by the experiment was repeated 5 times, as shown in Fig. 7, which was used to generate a 10-second time history.

5 Response analysis results

Modal analyses were first performed for the flat kerf models and are presented below. The wind analysis results under both static and dynamic loads were compared for flat kerf and solid panel models considering the displacement (out of plane), stress (von Mises), and strain (in-plane maximum) response parameters. Because the tendency of demand was increased proportionally with the basic wind speed, the results for three different wind speeds (WSs) are presented herein, namely 35.76 m/s (WS1), 62.60 m/s (WS2), and 82.73 m/s (WS3), representative of Category 1 (33-42m/s), Category 4(58-70 m/s) and Category 5 (>70 m/s) hurricane wind speeds, respectively. Response characteristics are presented in the following sections by panel type.

5.1 Modal analysis results

It is necessary to perform modal analysis on the kerf panels before determining their behavior under static and dynamic wind loadings. The resonance frequencies and mode shapes of the two kerf panels A and B with fixed edge boundaries were first determined as shown in Fig. 8 and 9, respectively. Both kerf panels undergo out-of-plane motion for the first few lower-order modes; however, their mode shapes are different. The kerf panel A being more flexible in the center shows higher curvature for the out-of-plane motion compared to the kerf panel B (see Mode 1 in Figures 7 and 8). The higher modes (>20) showed in-plane motion for both of the kerf panels. It can be concluded that the cut pattern affects both resonance frequencies and mode shapes. When designing kerf panels exposed to dynamic wind loading, it is necessary to avoid these natural frequencies. This study did not focus on local high-frequency responses of the panel which may be associated with air/wind passing through the kerfs because it is expected that such high-

frequency vibrations may induce cell resonances. Such a potential response should be investigated in future studies.

5.2 Static analysis results of flat kerf panels

289

290

291

292

293

294

295

296

297

298

299

300

301

302

303

304

305

306

307

308

309

310

311

The static loading was applied to all models of this study as described in Section 4. The results are reported in terms of out-of-plane displacement, maximum in-plane strain, and von Mises stress. Based on the results presented in Fig. 10 for WS2 (similar response observed for WS1 and WS3 as shown in Appendix A), the flexible kerf panels have higher displacement demands than the conventional type of solid panel. Different kerf patterns result in different displacement configurations, and hence different response characteristics of strains and stresses across the panels. While small strain response was shown in the center of Panel A, at the same region, high strain levels appeared in Panel B. These response characteristics were governed by the cut density, where higher cut density results in more flexible behaviors compared to lower cut density. The stress contours show similar response characteristics to the strain contours. From the stress response contour, a high-stress response for both kerf panels is generated at the connection areas between each unit cell. Also, from the stress response of Panel B, when the high-cut density region (the center region in the panel) undergoes a high level of deformation, a high degree of stress appears not only in the connection area but also in the center of the unit cell as well. The solid panel responds to the loading by resisting the force due to its relatively high stiffness and hence results in a smaller amplitude of displacement. On the other hand, in the kerf panels, cutting has reduced the overall stiffness of the panels and decreased the load-bearing ability. However, the flexibility of the kerf panels leads to different response mechanisms when subjected to loading. The kerf panels, being compliant, deform easily with loading by reconfiguring their shapes, as seen in relatively large out-of-plane displacements compared to the solid panel while the stresses

remain relatively small. From the simulation, the maximum stress developed is still slightly below the modulus of rupture (MOR) of the material. From the static analyses, it can be concluded that it is possible to alter the response characteristics of strains and stresses in the panels through arrangements of kerf patterns with different cut densities, which can be an advantage in minimizing or even mitigating damages in the panel when exposed to mechanical loading.

5.3 Static analysis results of pre-deformed kerf panels

To further investigate the response characteristics of kerf panels based on the degree of initial deformation, each "flat" panel (including kerf panels and solid panels) was modified to reflect an initial curvature. The curvatures of the "flat" models were modified so that the center of the curved panel had a distance of 50.08 mm, 101.6 mm, and 203.2 mm from the initially flat surface. All geometrical and material properties of the unit cell composed of the panel remained the same as for the flat panel models as well as the boundary conditions. Results are presented for the predeformed panel with a 101.6 mm distance from the flat surface and under WS2, while the remaining responses are shown in Appendix A.

Fig. 11 shows the out-of-plane displacement, maximum in-plane strain, and von Mises stress of the pre-deformed panels under WS2. When compared to the responses of flat panels, the pre-deformed panel A and solid panel show a smaller magnitude of displacement, strain, and stress under the same wind speed, while the pre-deformed kerf panel B exhibits more severe displacement, strain, and stress when compared to the flat kerf panel B. However, the stress magnitude is still lower than the MOR of the material (Table 2).

5.4 Dynamic analysis results of flat shape panels

Dynamic analysis results had a similar trend with the static analysis findings, as graphically shown in Fig. 12-14 for WS2 (WS1 and WS3 are presented in Appendix X). The contour results

for each structural response were summarized at 2.5-second intervals from 0 to 10 seconds, where the responses oscillate. Similar to the static analysis results, the displacement of the kerf panel A at the center region is relatively small owing to the low cut density region, while for the kerf panel B the high cut density at the center region yields to relatively large displacement. The displacements and strains in the solid panel are significantly low compared to the ones of the kerf panels. In the solid panel model during the oscillation, the location of the maximum strain value appeared to alter between the edge and center depending on the time history. For the kerf panel B, the maximum strain response appeared at the center location of the panel particularly at the center of the unit cell, while for the kerf panel A the maximum strains occurred close to the supports (edges) and/or along the regions with medium density cut. When observing the stress demands, the kerf panel A had significantly low stresses throughout the whole plate except for the medium cut density region, while the kerf panel B showed relatively larger stresses at the center region. However, the stress magnitude in all cases is lower than the MOR. The same response characteristics were observed in the panels under different wind speeds (WS1 and WS3), as shown in Appendix A.

5.5 Dynamic analysis results of pre-deformed shape panels

335

336

337

338

339

340

341

342

343

344

345

346

347

348

349

350

351

352

353

354

355

356

357

Responses of pre-deformed kerf panels under dynamics analysis were also investigated. The pre-deformed panels have the center at a distance of 50.8 mm, 101.6 mm, and 203.2 mm from the initially flat surface. All geometrical and material properties of the unit-cell composed of the panel remained the same as for the flat panel models as well as the boundary conditions.

Similarly, to the flat panels, the results for WS2 (Fig. 15-23) are presented herein, while the results for WS1 and WS3 are summarized in the Appendix A. By increasing the pre-deformation curvature, the out-of-plane displacements for kerf panel A under the same wind speed were

reduced, while for the kerf panel B, the out-of-plane displacement increased with increasing the curvatures. In kerf panel B, higher displacements were observed at the center of the panel, associated with high-density cut, while for panel A the locations of maximum displacements varied between the center and along the region with medium-density cut. In terms of strain and stress demands, a similar trend as in the displacement was observed. However, for the kerf panel B, the region of the maximum strains varied between the center region with high-density cut and the region with medium-density cut. For example, in the 101.6 mm initial curvature model of the kerf panel B, the highest strain demand was observed at the transition section (medium cut density) of unit cells, while in the 203.2 mm initial curvature model, the largest strain response occurred in the center (high cut density). It was also observed that in both kerf panels, the stress response occurred largely at the connection regions between unit cells. Overall, pre-deforming kerf panels with different degrees of curvatures alter both the stress and strain wave patterns from those of the flat-shaped kerf panels. Different levels of initial curvature can enhance the performance of the kerf panels, i.e., in panel A, with advantages in the design of building facades with complex shapes. The magnitude of displacement, stress, and strain in the kerf panels are relatively high compared to the solid panel, but they are still under safe design limits.

6 Discussion and Conclusions

358

359

360

361

362

363

364

365

366

367

368

369

370

371

372

373

374

375

376

377

378

379

380

This study investigates the response of kerf panels with different arrangements of cut densities subjected to strong wind loads through a series of static and dynamic analyses, while also comparing their structural performance to conventional construction material (solid panels). Responses of flat panels and pre-deformed panels (dome shapes) with different degrees of curvatures exposed to different wind speeds were studied. Three different loading conditions with wind speeds of 35.76 m/s, 62.60 m/s, and 82.73 m/s were considered to cover a variety of wind

loads per the Saffir-Simpson hurricane scale. These wind speeds are associated with hurricane categories 1, 4, and 5, respectively.

Based on the analysis results for the panel models, the solid panel was observed to resist the force due to its relatively high stiffness resulting in smaller displacement amplitudes, and hence smaller strains and stresses compared to those exhibited in the kerf panels. On the other hand, the kerf panels have reduced overall stiffness due to the cutting which further decreased their load-bearing ability. However, the kerf panel flexibility contributed to deforming easily with loading by global and local cell deformations and resulting in stress reduction within the cells, which may reduce potential damage due to overstress in the structures even when their load-bearing ability is less than the one of the solid panels. For the pre-deformed kerf panels with initial curvature of varying magnitudes, it was observed that both the overall stress and strain responses in certain kerf cut arrangements were lower than those of the flat-shaped panels. These modifications are attributed to changes in the overall stiffness of the pre-deformed kerf panels compared to the flat kerf panels and changes in wind pressure boundary conditions on kerf surfaces. The kerf panels can manipulate regions of extreme stresses and strains by altering the arrangements of the cut densities across the panels and/or by globally deforming them.

The kerf panels exhibited an enhanced performance overall as they minimized the exposure of external loads by compliant deformations. Additionally, the air gaps in the kerf panels allow the air to flow through them reducing the wind pressure effect on the panels. The flexibility and more compliant nature of the kerf panels enable configuring them into complex shapes achieving the desired freeform geometries from the architectural design standpoint. This study shows the promise of the use of kerf panels in achieving both design flexibility and performance demands when exposed to service loadings, i.e., wind exposures at various speeds.

This is a new proposed architectural configuration (design paradigm) for façades that could revolutionize structural engineering by pushing complex freeform shapes to a standard practice that intertwines aesthetic arguments, building performance requirements, and material design considerations, however, certain practical design aspects from a structural engineering perspective need to be addressed before full implementation of this design. The present study is the first one looking into the proposed architectural consideration for wind mitigation applications, however, certain limitations should be addressed as part of future research. More specifically, further studies are needed to focus on experimental investigations of these kerf panel designs (e.g., including wind tunnel tests) and be able to directly use the dynamic loading profile associated with kerf patterns of the studied panels for additional numerical investigations. Numerical simulations could also be further enhanced by evaluating the response/capacity of kerf panels using dynamic loading patterns available in databases other than the one considered herein (e.g., DesignSafe TTU WERFL building experiments, and FIU WoW experiments, TPU Aerodynamic database, NIST Aerodynamic database). Additionally, aeroelastic effects are not accounted for in the analyses presented in this paper. Future investigation on the interplay between the pattern of unit-cell, size of unit cell, size of panel, kerf pattern arrangements, materials used, and deformed configurations of the kerf panels is necessary to enhance our understanding of the performance characteristics of the kerf panels.

7 Acknowledgments

404

405

406

407

408

409

410

411

412

413

414

415

416

417

418

419

420

421

422

423

424

425

426

427

This study is funded by the US National Science Foundation (NSF) under Award No. CMMI 1912823 and 1913688. Any opinions, findings, conclusions, and recommendations presented in this paper are those of the authors and do not necessarily reflect the views of NSF. This financial support is greatly appreciated. The finite element analyses were conducted at Texas A&M's High-Performance Research Computing Center. This support is gratefully acknowledged.

References

- 429 Amini, M.O., and Van De Lindt, J.W. (2014). Quantitative insight into rational tornado design wind speeds 430 for residential wood-frame structures using fragility approach. *Journal of Structural Engineering* 431 140, 04014033.
- 432 An, G. (2016). *Integrated wind load combination and stiffness design optimization of irregular tall buildings*. Master of Philosophy M.Phil., The Hong Kong university of Science and technology.
- Andrade, D., Harada, M., and Shimada, K. (2017). Framework for automatic generation of facades on freeform surfaces. *Frontiers of Architectural Research* 6, 273-289.
- 436 Asce (2016). "Minimum Design Loads for Buildings and Other Structures". (Reston, VA: American Society of Civil Engineers).
- Blake, E.S., Rappaport, E.N., Jarrell, J.D., and Landsea, C. (2005). The deadliest, costliest, and most intense United States tropical cyclones from 1851 to 2004 (and other frequently requested hurricane facts).
- Blake, E.S., Rappaport, E.N., Jarrell, J.D., and Landsea, C. (2011). The deadliest, costliest, and most intense
 United States tropical cyclones from 1851 to 2010 (and other frequently requested hurricane facts).
- Boustan, L.P., Kahn, M.E., Rhode, P.W., and Yanguas, M.L. (2020). The effect of natural disasters on economic activity in US counties: A century of data. *Journal of Urban Economics*, 103257.
- Casaburo, A., Petrone, G., Franco, F., and De Rosa, S. (2019). A review of similitude methods for structural engineering. *Applied Mechanics Reviews* 71.
- Chan, C.M., Huang, M., and Kwok, K.C. (2010). Integrated wind load analysis and stiffness optimization of tall buildings with 3D modes. *Engineering structures* 32, 1252-1261.
- Chen, R. (2018). Attaining Desired Deformations of Flexible Structures through Mechanical and Non-Mechanical Stimuli. MASTER OF SCIENCE Master's thesis, Texas A&M University.
- Chen, R., Turman, C., Jiang, M., Kalantar, N., Moreno, M., and Muliana, A. (2020). Mechanics of kerf patterns for creating freeform structures. *Acta Mechanica*, 1-26.
- Chen, Z., and Chui, Y.-H. (2017). Lateral load-resisting system using mass timber panel for high-rise buildings. *Frontiers in Built Environment* 3, 40.
- Darnal, A., Shahid, Z., Han, J., Moreno, M., and Muliana, A. (Year). "Viscoelastic responses of MDF kerf structures", in: *Proceedings of the American Society for Composites—Thirty-Sixth Technical Conference on Composite Materials*).
- Doan, T.L., and Nguyen, T.G. (2019). Dynamic analysis of the laminated composite plate resting on twoparameter elastic foundation subjected to moving mass using finite element method. *Journal of Science and Technique* 14.
- Dung, N.T., Minh, P.V., Hung, H.M., and Tien, D.M. (2021). The third-order shear deformation theory for modeling the static bending and dynamic responses of piezoelectric bidirectional functionally graded plates. *Advances in Materials Science and Engineering* 2021, 1-15.
- Eekhout, M. (2016). Free Form Technology from Delft. IOS Press.
- Eigensatz, M., Kilian, M., Schiftner, A., Mitra, N.J., Pottmann, H., and Pauly, M. (2010). "Paneling architectural freeform surfaces," in *ACM SIGGRAPH 2010 papers*.), 1-10.
- 466 Epa (2016). Climate Change Indicators: Tropical Cyclone Activity [Online]. Available:
 467 https://www.epa.gov/climate-indicators/climate-change-indicators-tropical-cyclone-activity
 468 [Accessed].
- 469 Finn, D. (2017). CHAIN LINK FENCE MANUFACTURERS INSTITUTE PRODUCT MANUAL.
- 470 Finn, D. (2018). CHAIN LINK FENCE WIND LOAD GUIDE FOR THE SELECTION OF LINE POST 471 AND LINE POST SPACING.

- 472 Guzelci, O.Z., Alaçam, S., and Bacınoğlu, S.Z. (2017). Three-step experimentation on embedding curvature 473 to rigid planar materials through cut patterns. Gestão & Tecnologia de Projetos 12, 93-107.
- 474 Ha, J., Jung, S., Baek, H., Lee, H., and Nguyen, K.T. (2014). Analysis of Form and Space Changes in 475 Design Process of Freeform Architecture of Culture-Related Facilities in South Korea. 476 Architectural research 16, 157-166.
- 477 Harris, H.G., and Sabnis, G. (1999). Structural modeling and experimental techniques. CRC press.
- 478 He, J. (2018). System Nonlinear Performance of Low-Rise Buildings under Database-Assisted Hurricane 479 Loads. PhD Dissertation, Louisiana State University and Agricultural & Mechanical College.
- 480 He, J., Pan, F., Cai, C., Chowdhury, A., and Habte, F. (2018). Progressive failure analysis of low-rise timber 481 buildings under extreme wind events using a DAD approach. Journal of Wind Engineering and 482 Industrial Aerodynamics 182, 101-114.
- 483 Holterman, A. (2018). Pattern Kerfing for Responsive Wooden Surfaces: A formal approach to produce 484 flexible panels with acoustic performance. MSc Architecture, Urbanism and Building Sciences 485 Master's thesis, Delft University of Technology.
- 486 Jafari, M., and Alipour, A. (2020). Methodologies to mitigate wind-induced vibration of tall buildings: A 487 state-of-the-art review. Journal of Building Engineering, 101582.
- 488 Kalantar, N., Borhani, A., and Akleman, E. (Year). "Nip and tuck: a simple approach to fabricate double 489 curved surfaces with 2d cutting", in: eCAADe), 344-337.
- 490 Kim, K., Son, K., Kim, E.-D., and Kim, S. (2015). Current trends and future directions of free-form building 491 technology. Architectural Science Review 58, 230-243.
- 492 Koliou, M., and Van De Lindt, J.W. (2020). Development of building restoration functions for use in 493 community recovery planning to tornadoes. Natural Hazards Review 21, 04020004.
- 494 Mooneghi, M.A., and Kargarmoakhar, R. (2016). Aerodynamic mitigation and shape optimization of 495 buildings. *Journal of building engineering* 6, 225-235.
- 496 (2020a). Billion-Dollar Noaa Weather and Climate Disasters [Online]. Available: 497 https://www.ncdc.noaa.gov/billions/ [Accessed July 9 2020].
- 498 Noaa (2020b). State of the Climate: Hurricanes and Tropical Storms for Annual 2019 [Online]. NOAA 499 Atmospheric (National Oceanic and Administration). Available: 500 https://www.ncdc.noaa.gov/sotc/tropical-cyclones/201913 [Accessed July 9 2020].
- 501 Tornadoes for Annual 2019 [Online]. Available: (2020c). State of the Climate: 502 https://www.ncdc.noaa.gov/sotc/tornadoes/201913 [Accessed 2020].
- 503 Noaa (2022). The 25 Deadliest U.S. Tornadoes [Online]. NOAA (National Oceanic and Atmospheric 504 Administration). Available: https://www.spc.noaa.gov/faq/tornado/killers.html [Accessed 2022].
- 505 Phung, M.V., Nguyen, D.T., Doan, L.T., Nguyen, D.V., and Duong, T.V. (2022). Numerical investigation 506 on static bending and free vibration responses of two-layer variable thickness plates with shear connectors. Iranian Journal of Science and Technology, Transactions of Mechanical Engineering 508 46, 1047-1065.
- 509 Pottmann, H., Liu, Y., Wallner, J., Bobenko, A., and Wang, W. (2007). "Geometry of multi-layer freeform 510 structures for architecture," in ACM SIGGRAPH 2007 papers.), 65-es.

- 511 Pottmann, H., and Wallner, J. (2016). Geometry and freeform architecture. Mathematics and Society, 131-512 151.
- 513 Raker, E.J. (2020). Natural hazards, disasters, and demographic change: The case of severe tornadoes in 514 the United States, 1980–2010. Demography, 1-22.
- 515 Reeves, R. (2015). Economic Losses and Extreme Tornado Events. Degree of Master of Science Master's 516 thesis, University of South Carolina.

- Saaed, T.E., Nikolakopoulos, G., Jonasson, J.-E., and Hedlund, H. (2015). A state-of-the-art review of structural control systems. *Journal of Vibration and Control* 21, 919-937.
- Shahid, Z., Bond, C.G., Johnson, M.S., Hubbard Jr, J.E., Kalantar, N., and Muliana, A. (2022a). Dynamic
 response of flexible viscoelastic kerf structures of freeform shapes. *International Journal of Solids* and Structures 254, 111895.
- 522 Shahid, Z., Hubbard, J.E., Kalantar, N., and Muliana, A. (2022b). An investigation of the dynamic response of architectural kerf structures. *Acta Mechanica*, 1-25.
- Shahid, Z., Johnson, M.S., Bond, C.G., Hubbard Jr, J., Kalantar, N., and Muliana, A. (Year). "Dynamic
 responses of architectural kerf structures", in: *Proceedings of the American Society for Composites—Thirty-Sixth Technical Conference on Composite Materials*).
- 527 Sharma, A., Mittal, H., and Gairola, A. (2018). Mitigation of wind load on tall buildings through aerodynamic modifications. *Journal of Building Engineering* 18, 180-194.
- 529 Simmons, K.M., Kovacs, P., and Kopp, G.A. (2015). Tornado damage mitigation: Benefit—cost analysis of enhanced building codes in Oklahoma. *Weather, climate, and society* 7, 169-178.
- 531 Simmons, K.M., Kovacs, P., and Smith, A.B. (2020). State-by-state analysis of benefits to cost from wind-532 enhanced building codes. *Natural hazards review* 21, 04020007.
- 533 Simmons, K.M., Sutter, D., and Pielke, R. (2013). Normalized tornado damage in the United States: 1950– 2011. *Environmental Hazards* 12, 132-147.
- 535 Simulia (2018). "ABAQUS/Standard Version 6.18 Analysis User's Manual". Pawtucket Rhode Island).
- 536 Son, S., Fitriani, H., Kim, J.T., Go, S., and Kim, S. (Year). "Mathematical algorithms of patterns for freeform panels", in: *Proceedings of the 2nd world congress on Civil, Structural, and Environmental* 538 Engineering (CSEE'17)), 1-8.
- 539 Standohar-Alfano, C.D., and Van De Lindt, J.W. (2016). Tornado risk analysis for residential wood-frame roof damage across the United States. *Journal of Structural Engineering* 142, 04015099.
- Ta, D.T., and Tran, V.K. (2020). Static bending analysis of symmetrical three-layer FGM beam with shear connectors under static load. *Journal of Science and Technique* 15.
- Zarrinmehr, S., Ettehad, M., Kalantar, N., Borhani, A., Sueda, S., and Akleman, E. (2017). Interlocked archimedean spirals for conversion of planar rigid panels into locally flexible panels with stiffness control. *Computers & Graphics* 66, 93-102.
- Zhu, Y., Wang, Y., Luo, Z., Han, Q., and Wang, D. (2017). Similitude design for the vibration problems of plates and shells: A review. *Frontiers of Mechanical Engineering* 12, 253-264.

Table 1: Dimension of unit-cell and computed effective area of kerf pattern panels

	Low cutting density unit- cell	Medium cutting density unit-cell	High cutting density unit- cell	Total area
Total Length in plane of each unit cell (mm)	171.16	275.29	377.91	-
Width (mm)	2.54	1.48	0.95	-
Depth (mm)	3.175	3.175	3.175	-
Area per cell (mm²)	434.75	407.65	359.96	-
Quantities in panel A	27	134	64	-
Quantities in panel B	104	72	49	-
Panel A (mm²)	-	-	-	9.22 E+04
Panel B (mm ²)	-	-	-	8.94 E+04

Table 2: Model and prototype domain properties

Model domain	Prototype domain	
381	1,219.20	
381	1,219.20	
3.18	3.18	
650.48	650.48	
390.52	3,998.96	
3.50	35.84	
0.25	0.25	
	381 381 3.18 650.48 390.52 3.50	



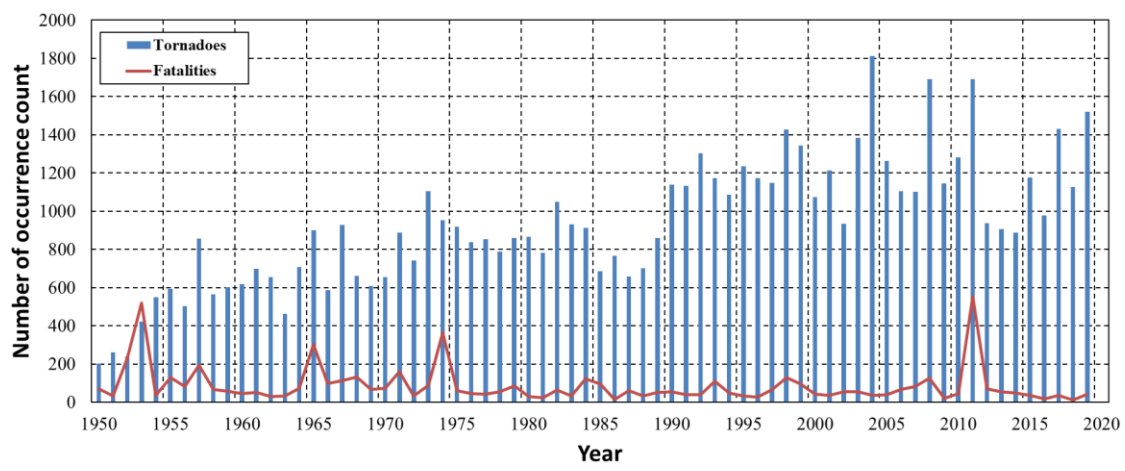


Fig. 1: Recorded tornadoes and fatalities per year in the United States (Data from (NOAA, 2020c))

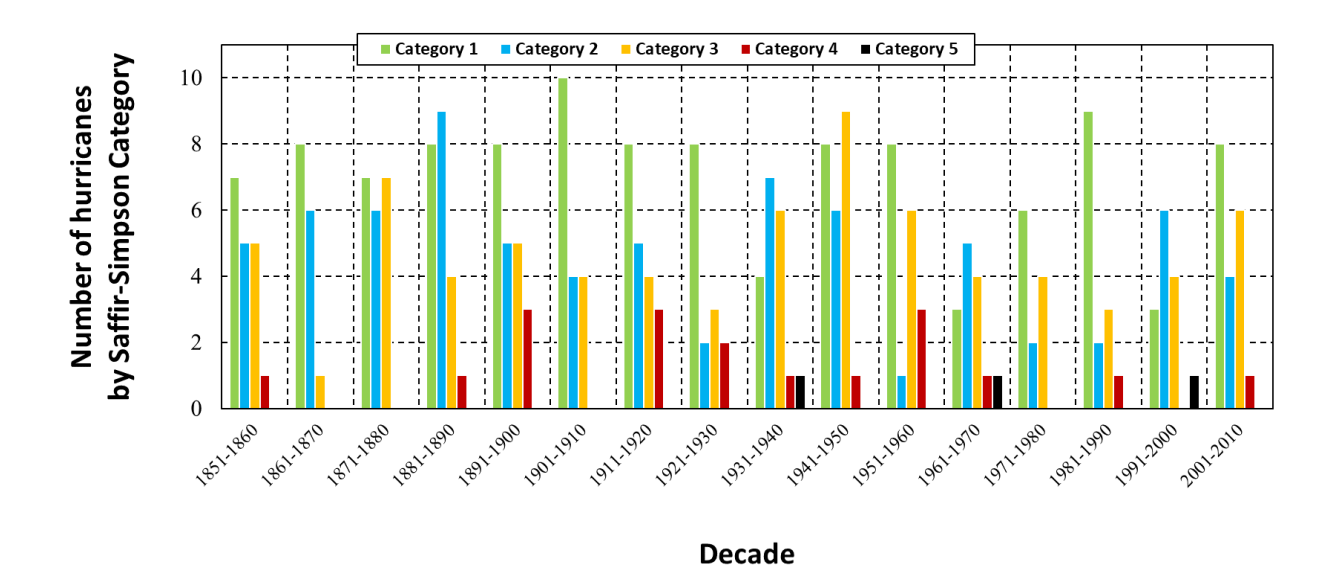


Fig. 2: Number of hurricanes by Saffir-Simpson Category to strike the United States each decade (Data from (Blake et al., 2011))

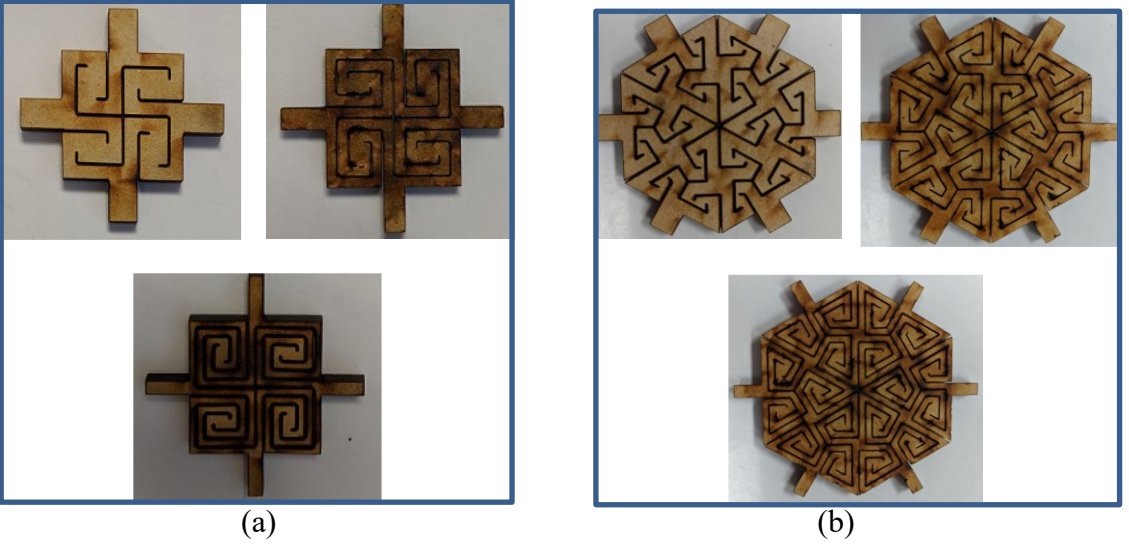


Fig. 3: Unit cells on the kerf pattern panel: (a) square kerf pattern, and (b) hexagon kerf pattern

(Chen et al., 2020)

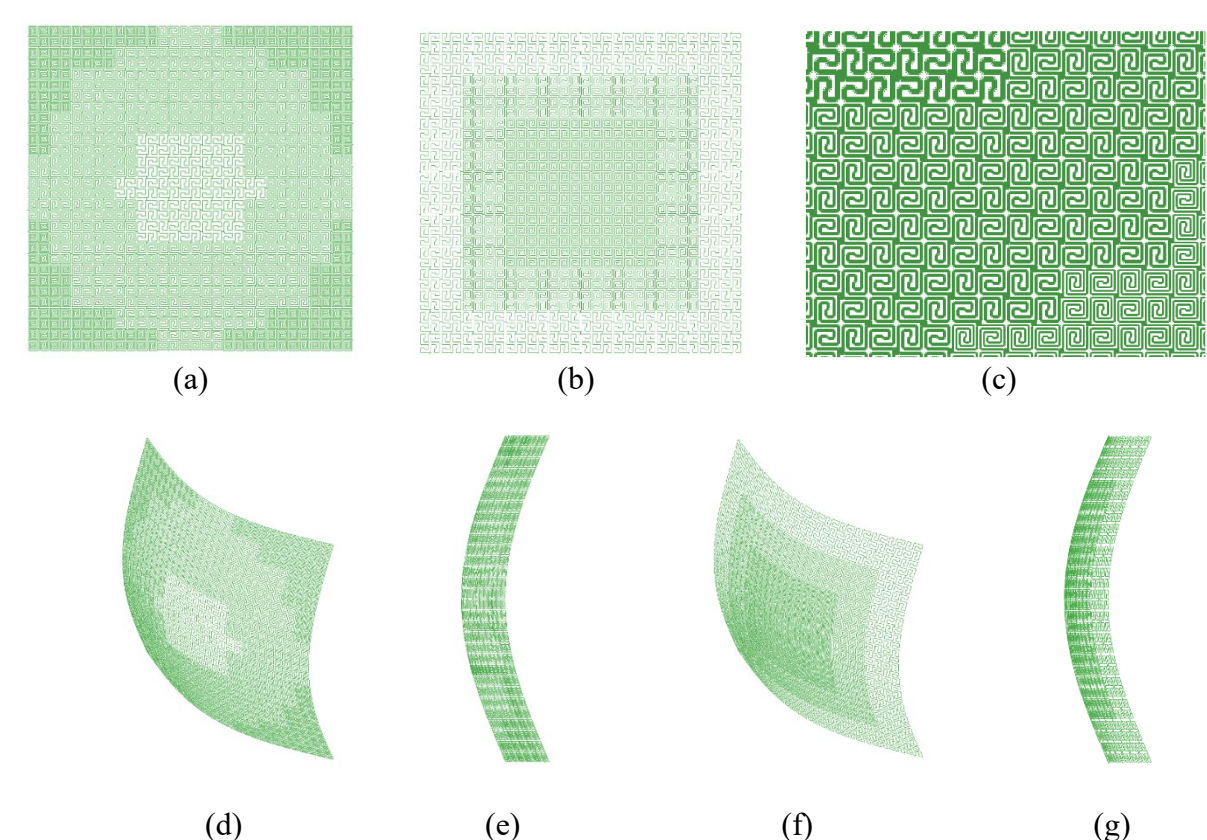
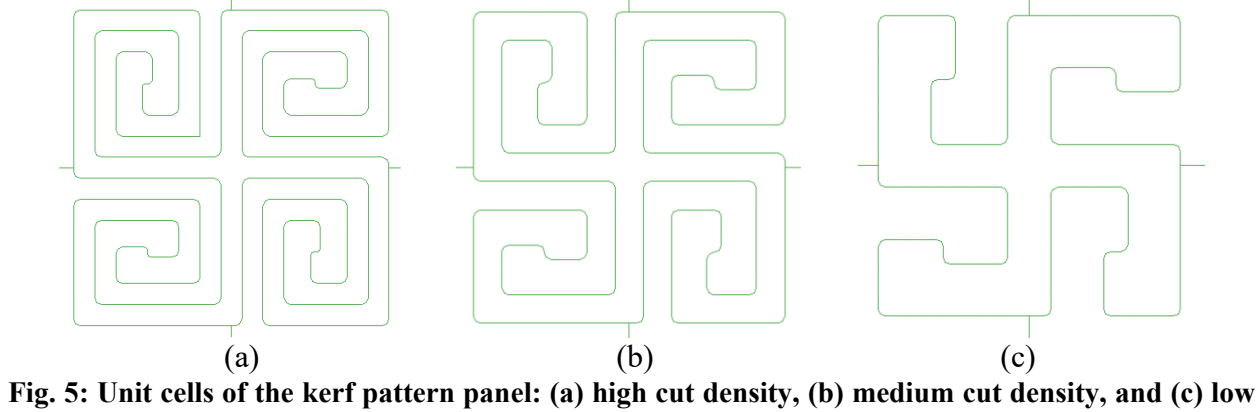


Fig. 4: Layout of the kerf panel finite element models: (a) flat panel A, (b) flat panel B, (c) enlarged unit-cell transition area, (d) isometric view of deformed panel A, (e) side view of deformed panel A, (f) isometric view of deformed panel B, and (g) side view of deformed panel B



cut density

567 568

569

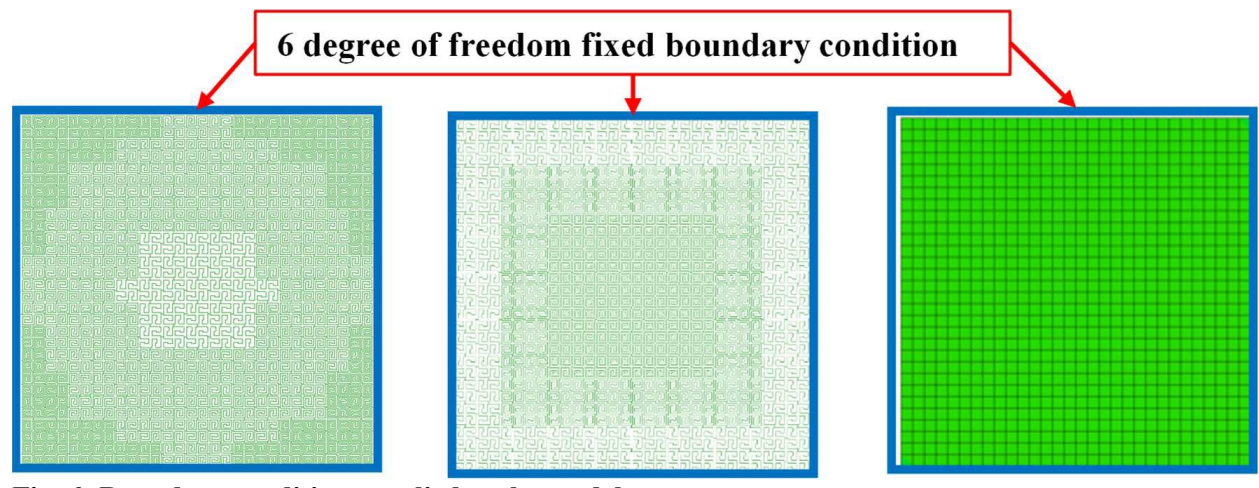


Fig. 6: Boundary conditions applied to the model

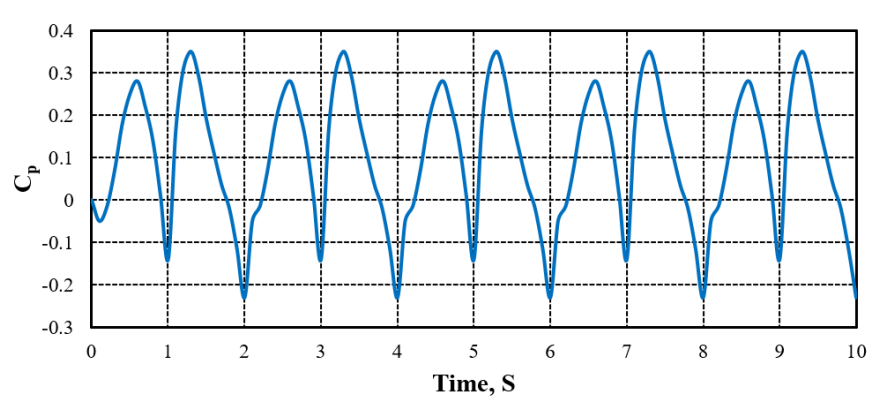


Fig. 7: Wind load coefficient time history (He et al., 2018)

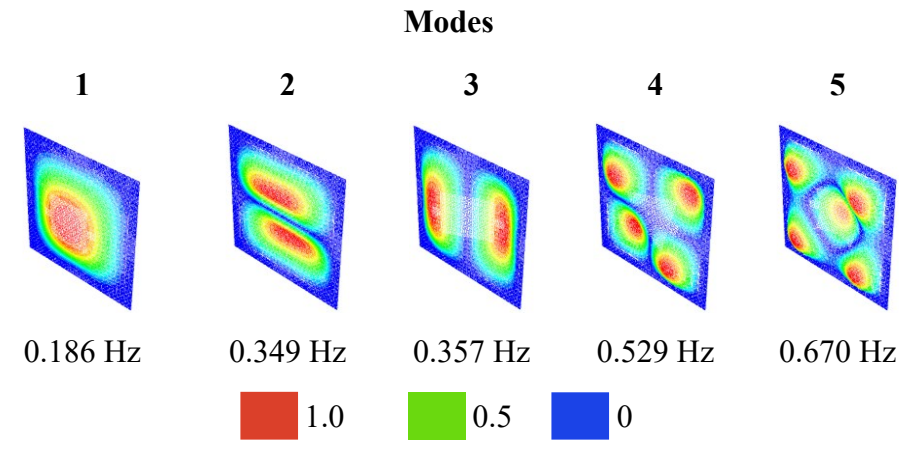


Fig. 8: Modal responses showing normalized displacement contours for kerf panel A

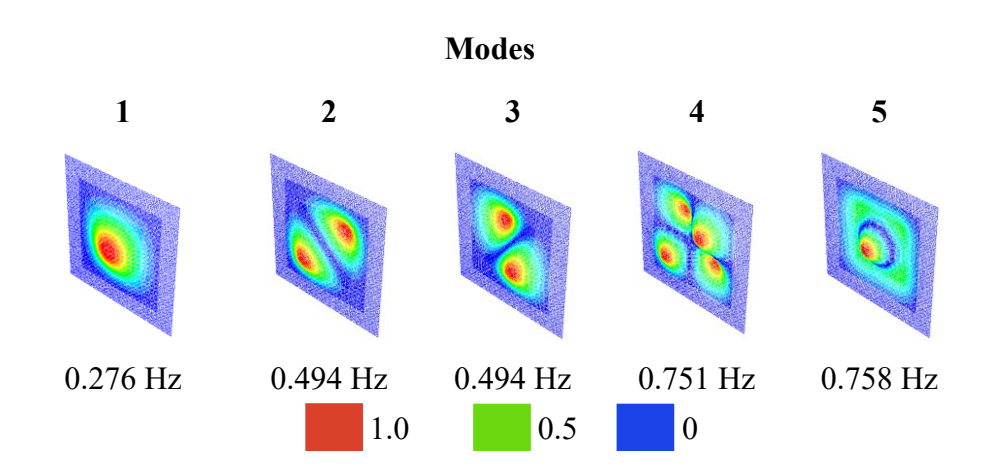


Fig. 9: Modal responses showing normalized displacement contours for kerf panel B

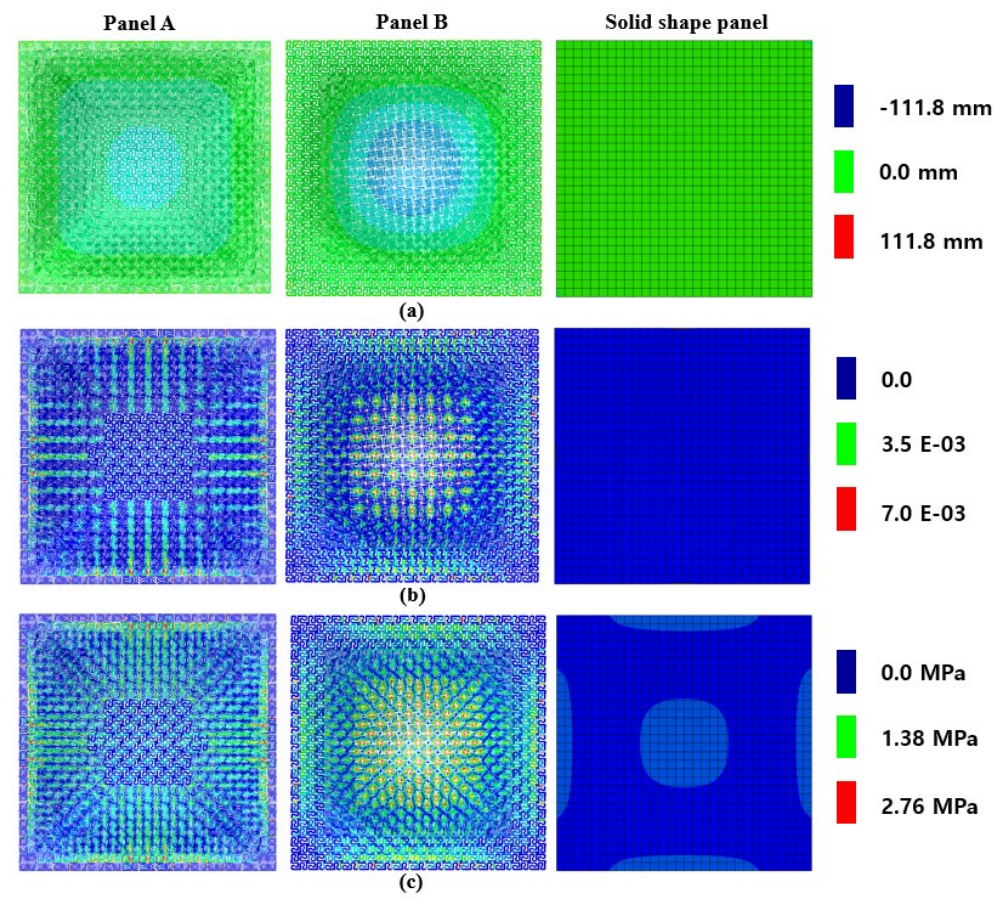


Fig. 10: Static analysis results for WS2: (a) displacement, (b) strain, and (c) stress

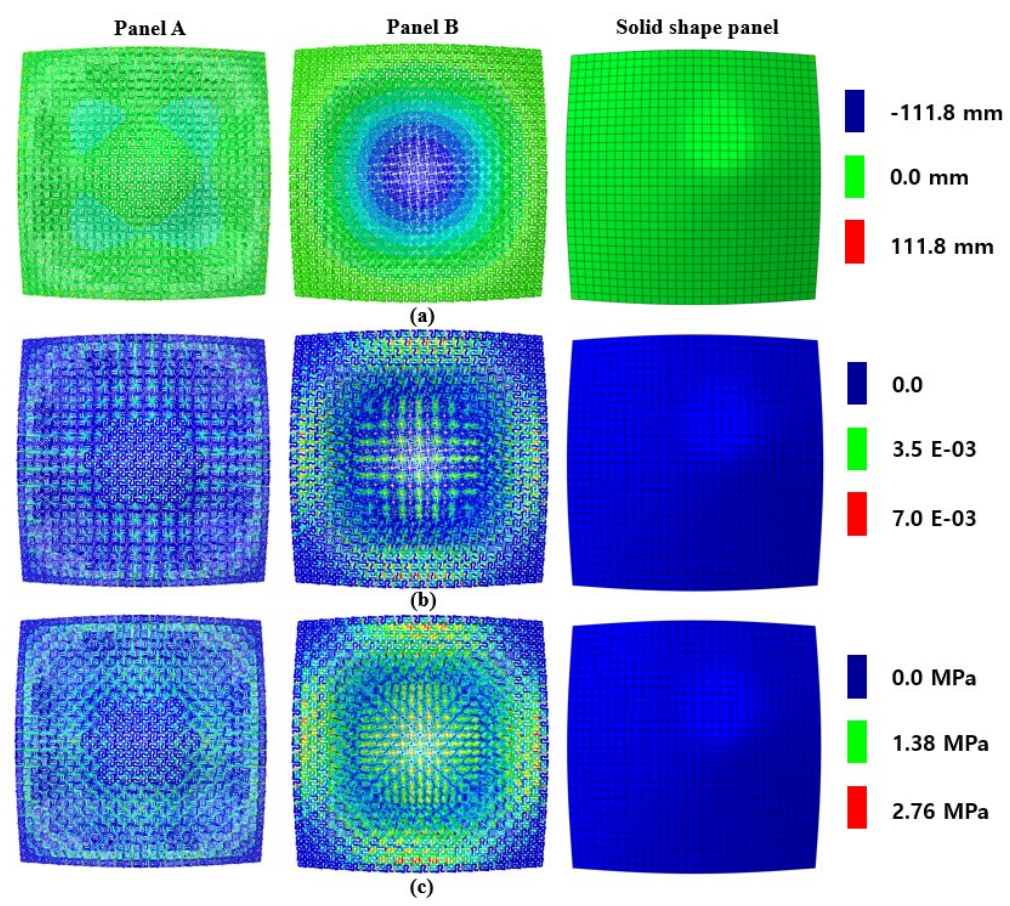


Fig. 11: Static analysis results of 10.16 cm pre-deformed shape panels for WS2: (a) displacement, (b)

582 strain, and (c) stress

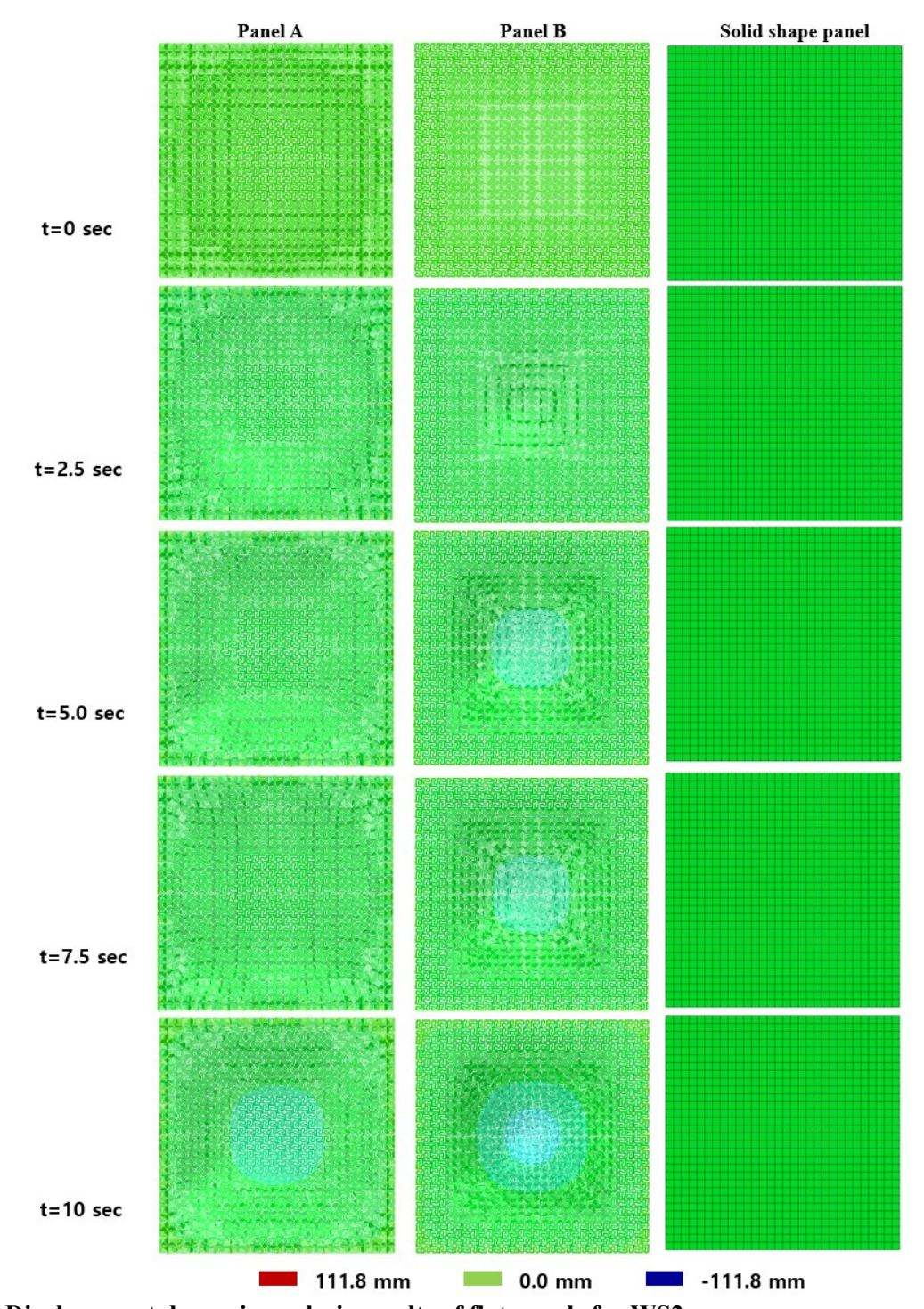


Fig. 12: Displacement dynamic analysis results of flat panels for WS2

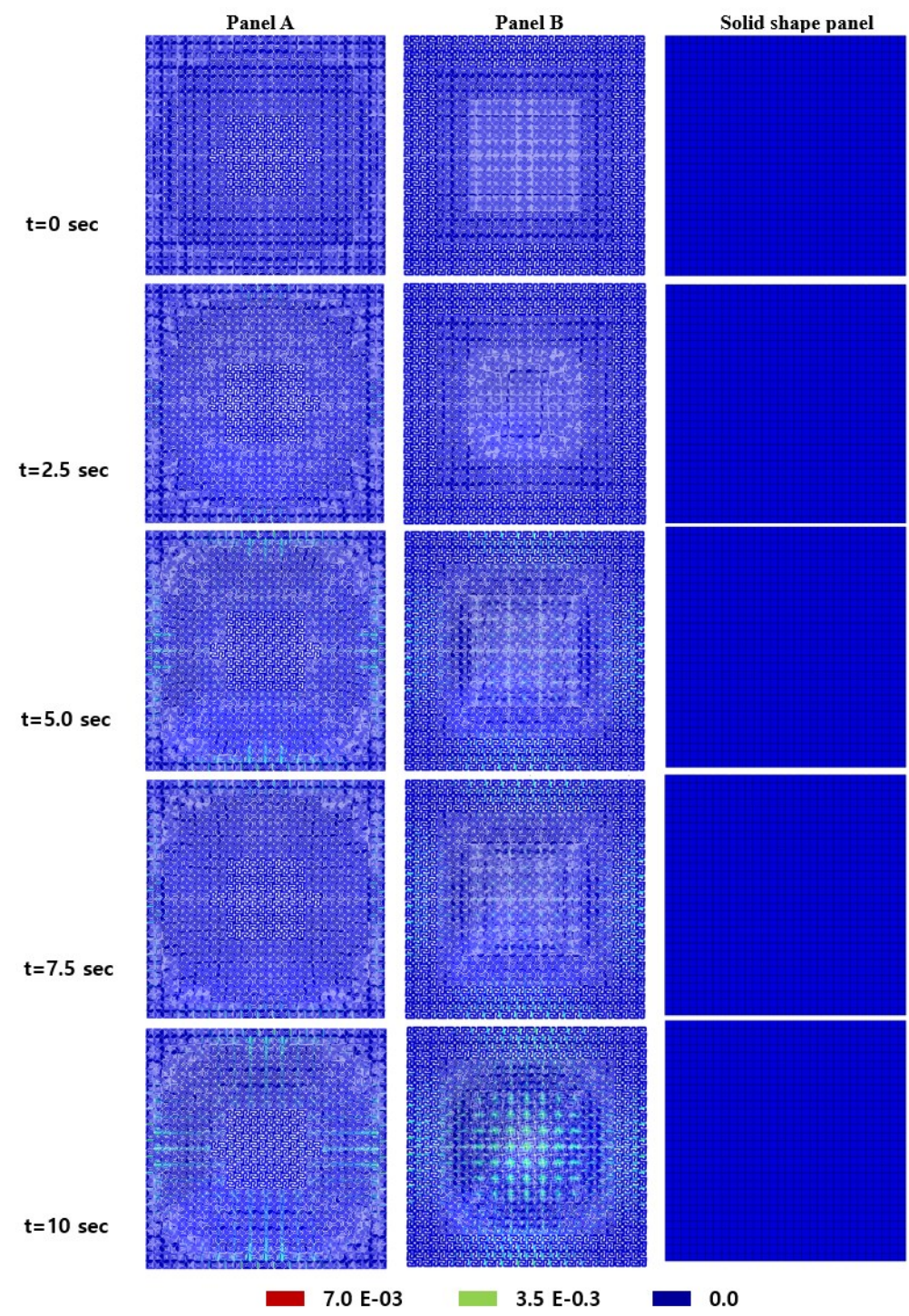


Fig. 13: Strain dynamic analysis results of flat panels for WS2

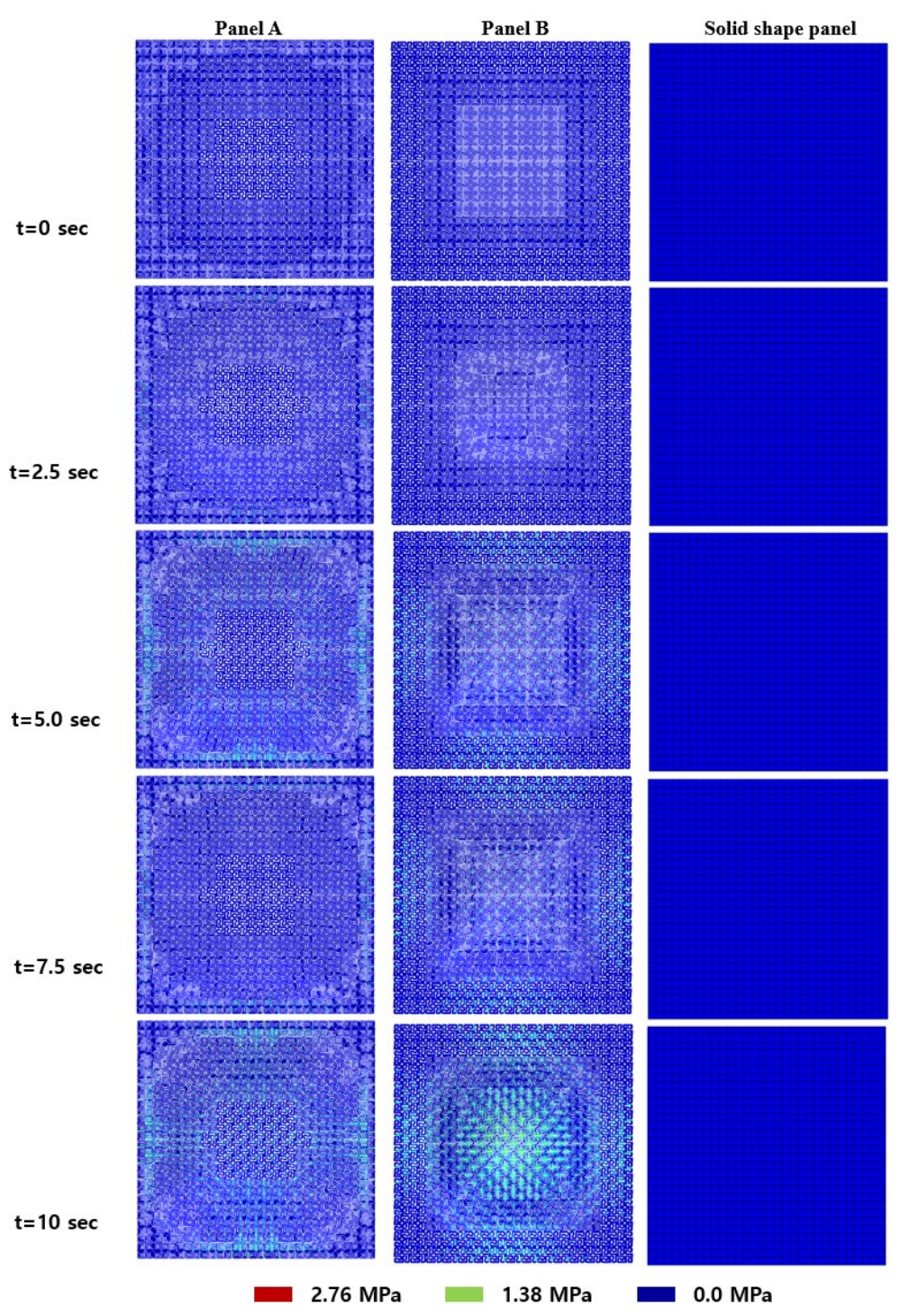


Fig. 14: Stress dynamic analysis results of flat panels for WS2

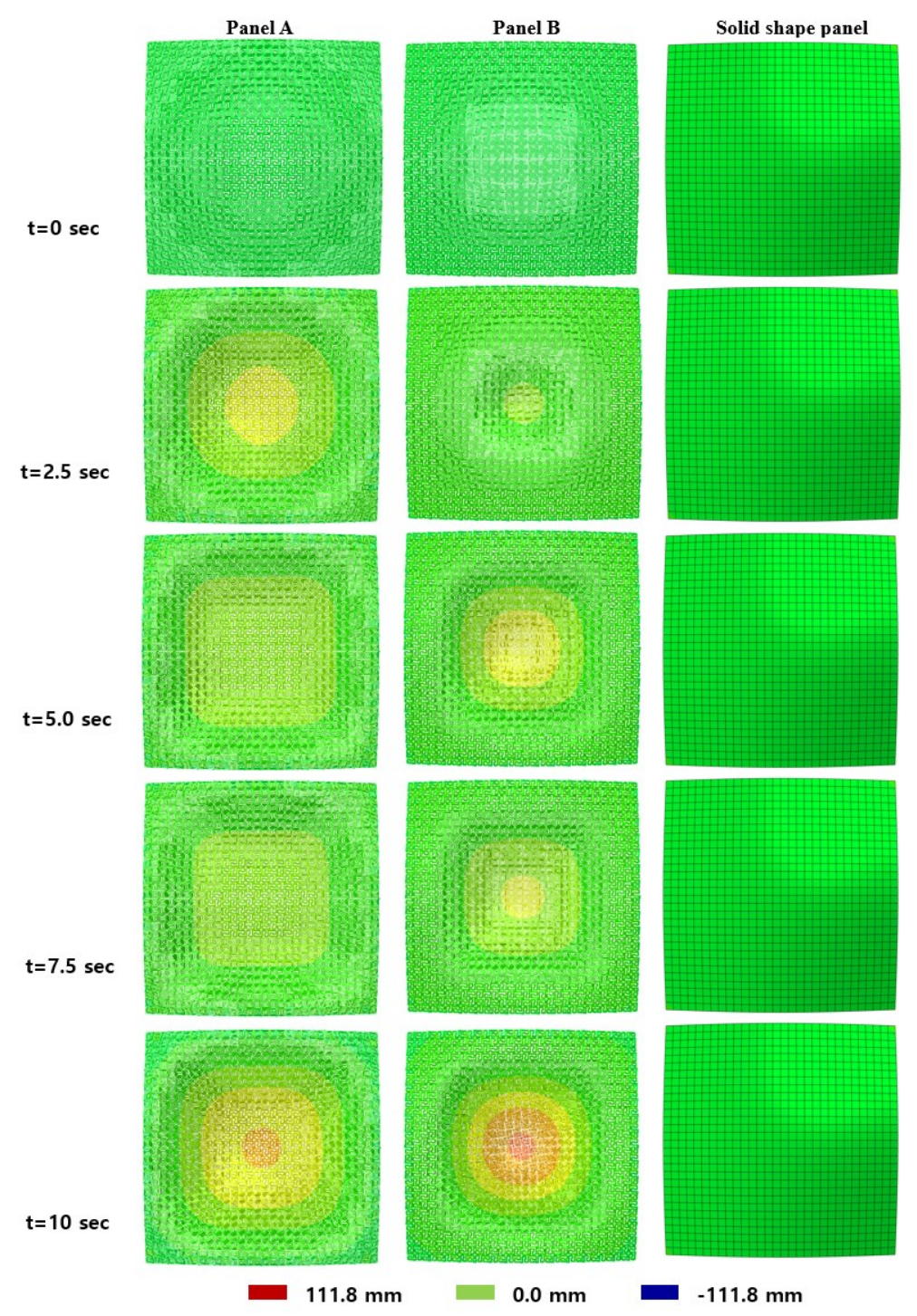


Fig. 15: Displacement dynamic analysis results of 50.8 mm pre-deformed shape panels for WS2

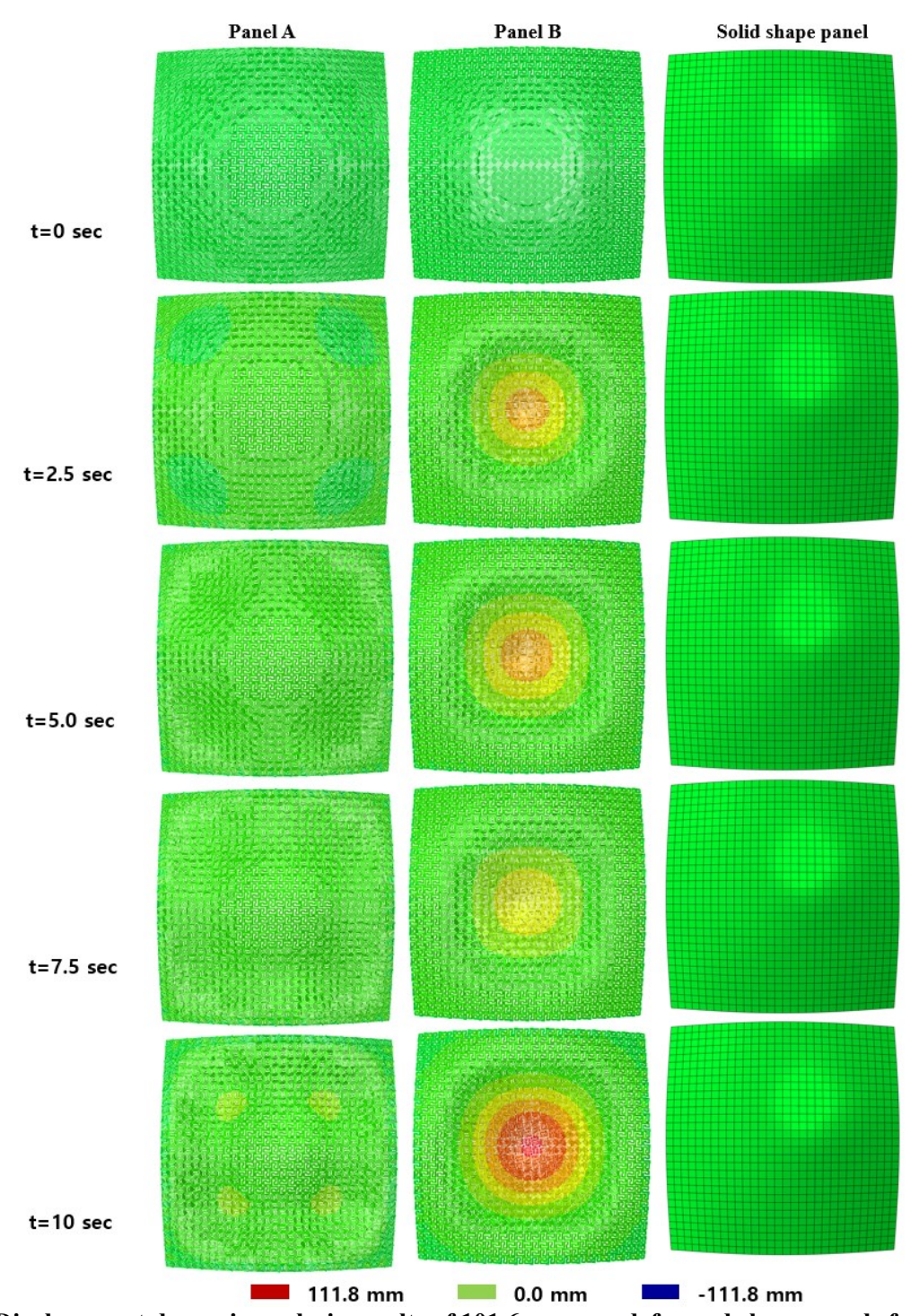


Fig. 16: Displacement dynamic analysis results of 101.6 mm pre-deformed shape panels for WS2

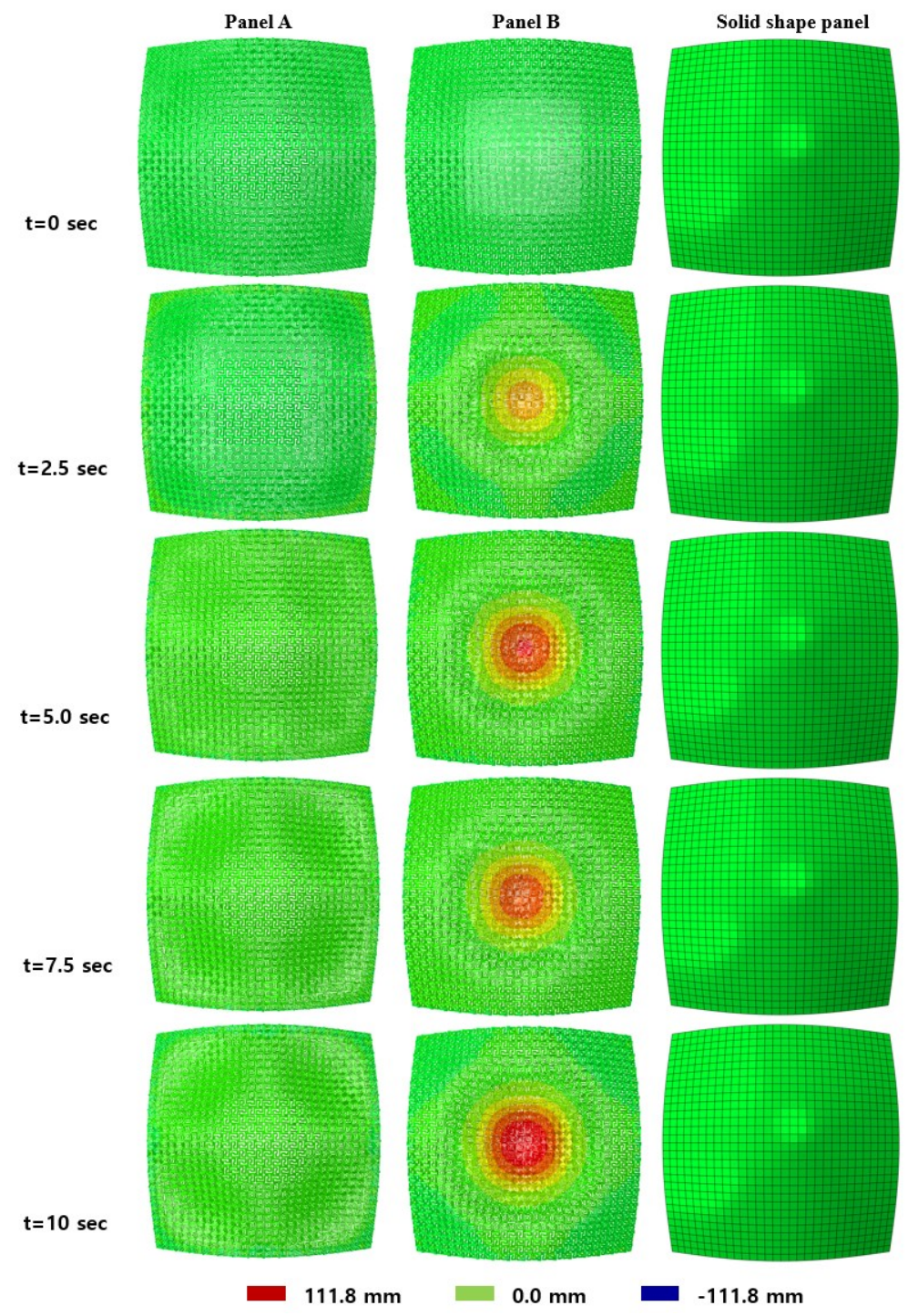


Fig. 17: Displacement dynamic analysis results of 203.2 mm pre-deformed shape panels for WS2

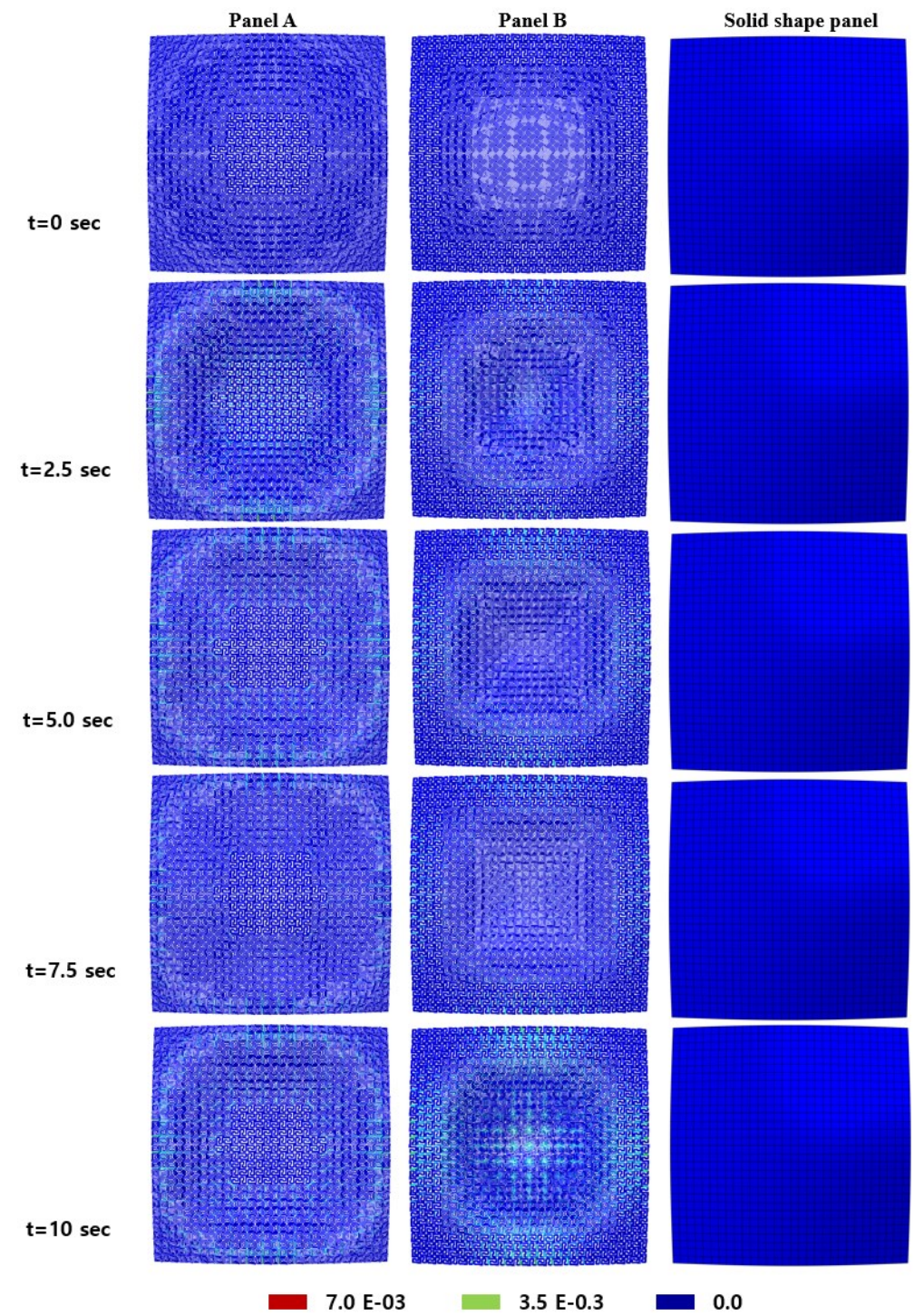


Fig. 18: Strain dynamic analysis results of 50.8 mm pre-deformed shape panels for WS2

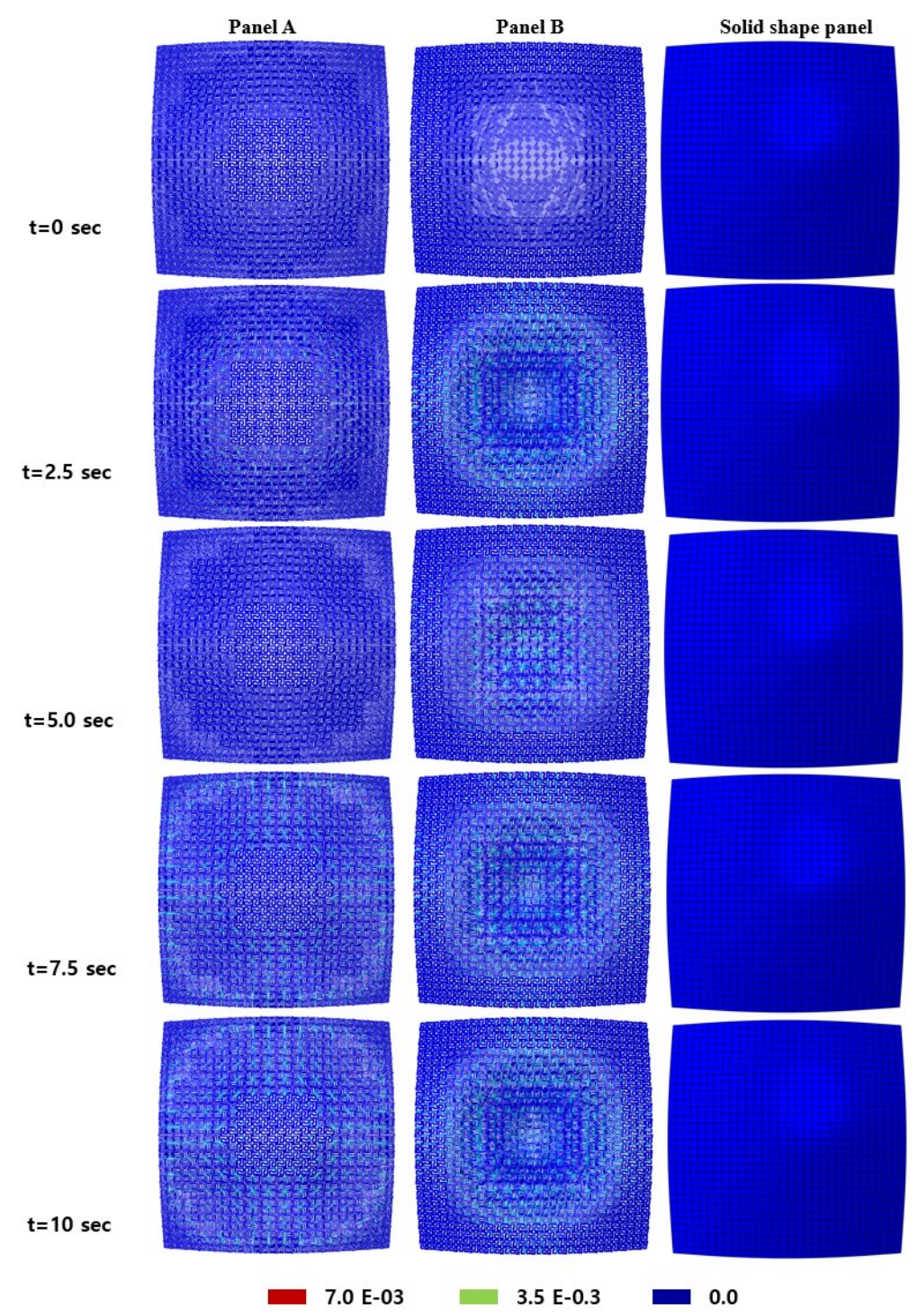


Fig. 19: Strain dynamic analysis results of 101.6 mm pre-deformed shape panels for WS2

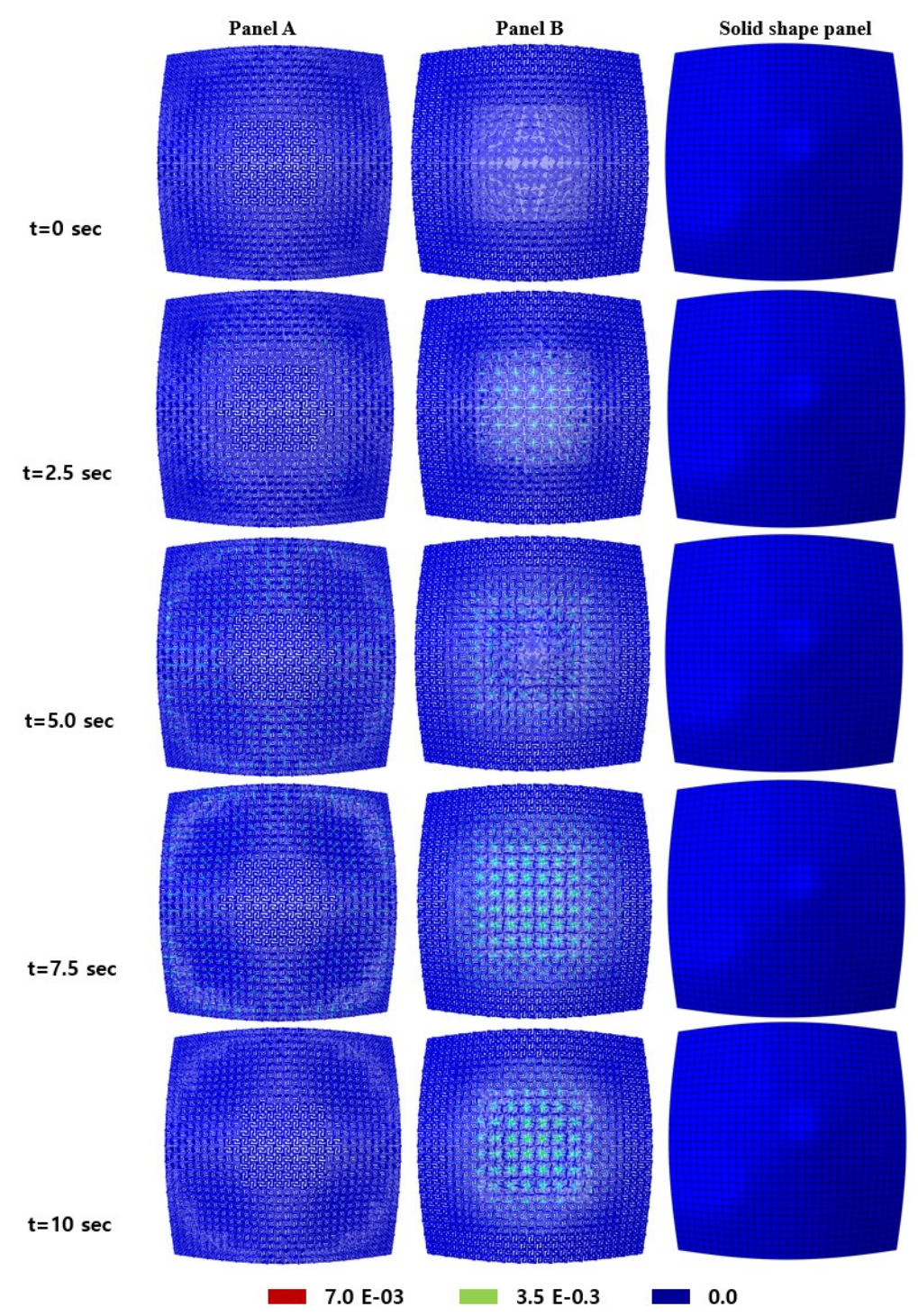


Fig. 20: Strain dynamic analysis results of 203.2 mm pre-deformed shape panels for WS2

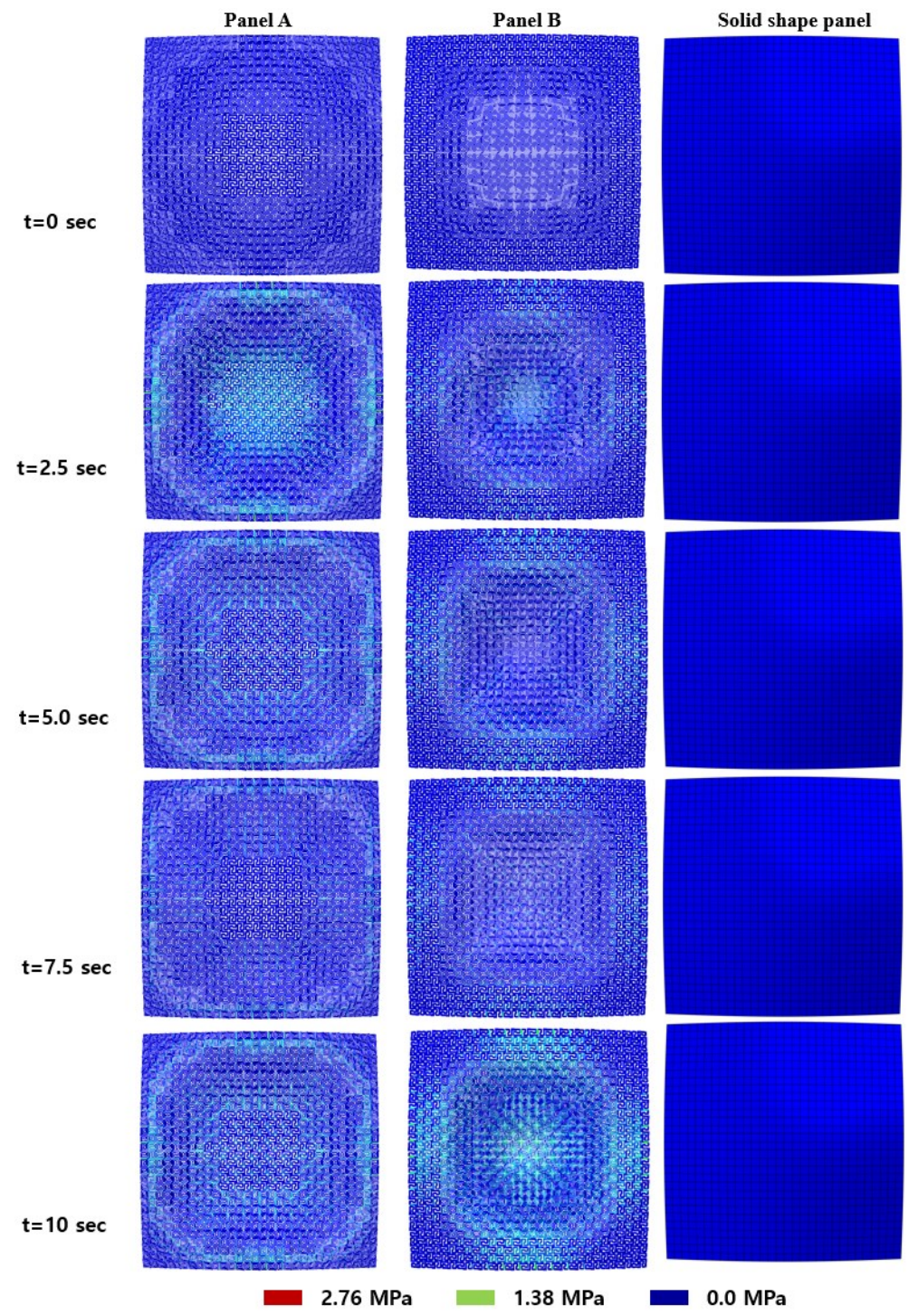


Fig. 21: Stress dynamic analysis results of 50.8 mm pre-deformed shape panels for WS2

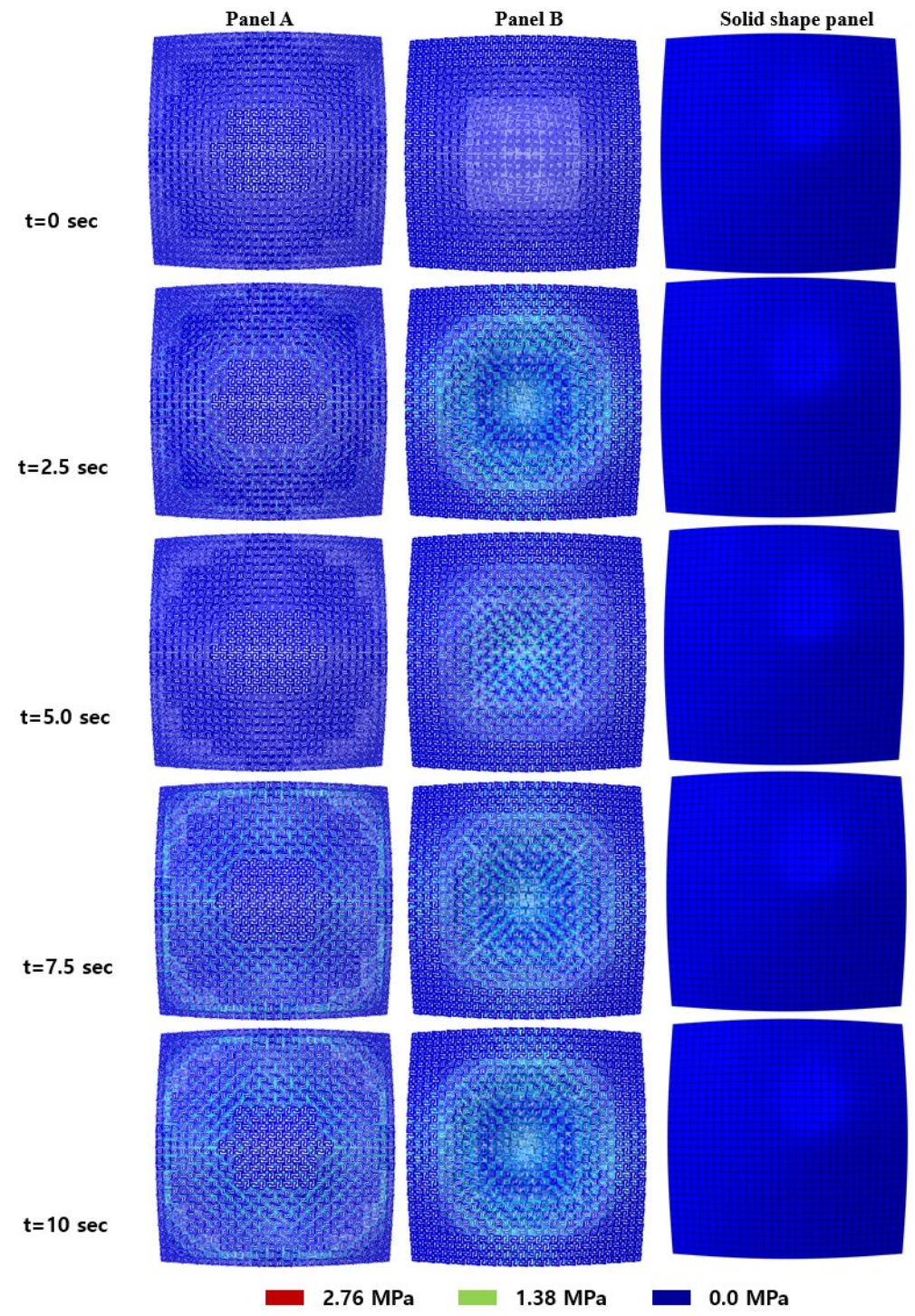


Fig. 22: Stress dynamic analysis results of 101.6 mm pre-deformed shape panels for WS2

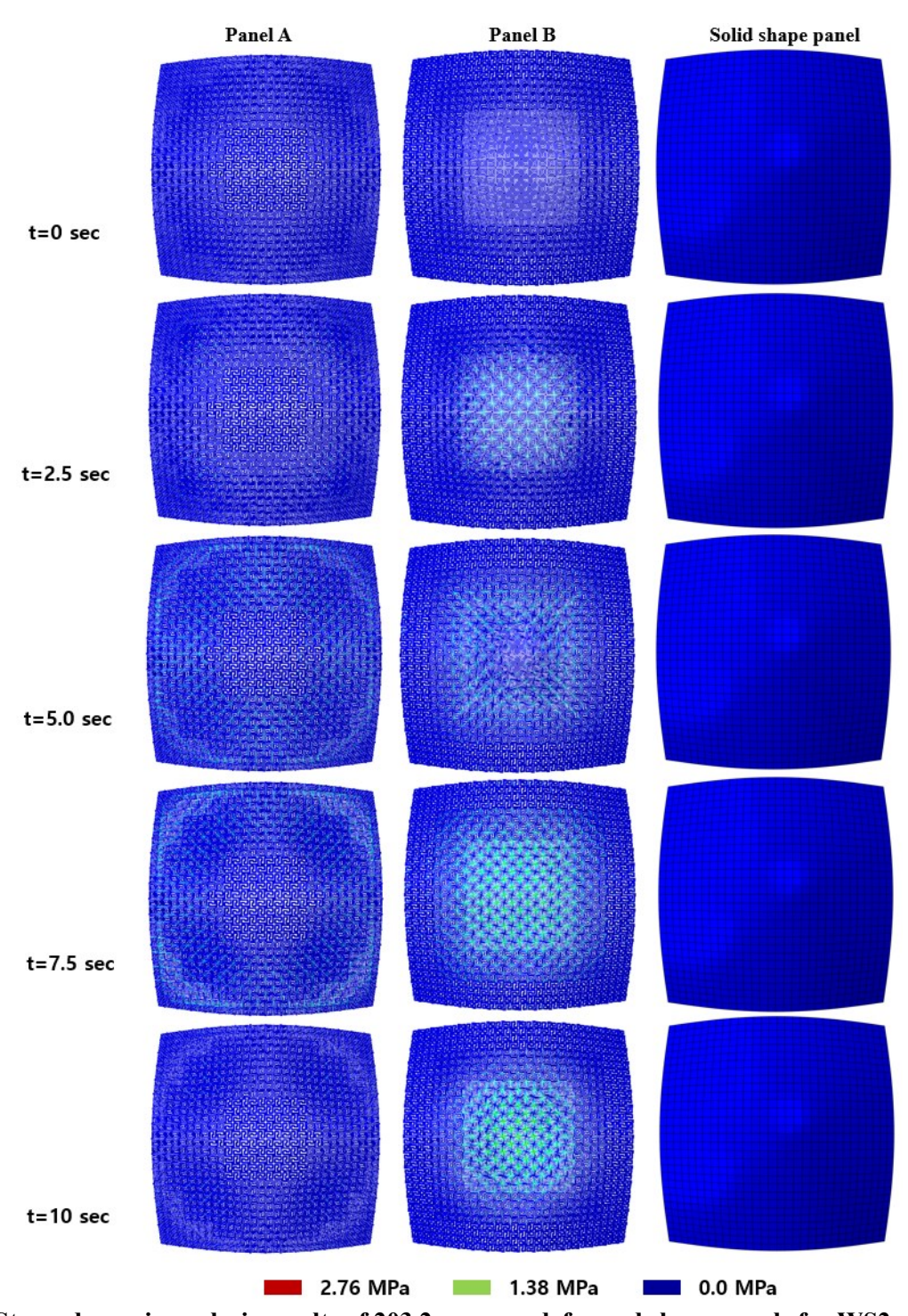


Fig. 23: Stress dynamic analysis results of 203.2 mm pre-deformed shape panels for WS2